Computers in Biology and Medicine 124 (2020) 103826

Contents lists available at ScienceDirect

Computers in Biology and Medicine

journal homepage: http://www.elsevier.com/locate/compbiomed

Inlet flow rate of perfusion bioreactors affects fluid flow dynamics, but not oxygen concentration in 3D-printed scaffolds for bone tissue engineering: Computational analysis and experimental validation

Hadi Seddiqi [a,1], Alireza Saatchi [a,b,1], Ghassem Amoabediny [a,b,c,*], Marco N. Helder [c], Sonia Abbasi Ravasjani [a], Mohammadreza Safari Hajat Aghaei [a], Jianfeng Jin [d], Behrouz Zandieh-Doulabi [d,2], Jenneke Klein-Nulend [d,2]

[a] Department of Biomedical Engineering, Research Center for New Technologies in Life Science Engineering, University of Tehran, Tehran, P.O. Box 11365-4563, Iran
[b] School of Chemical Engineering, College of Engineering, University of Tehran, P.O. Box 11365-4563, Tehran, Iran
[c] Department of Oral and Maxillofacial Surgery/Oral Pathology, Amsterdam University Medical Centers and Academic Centre for Dentistry Amsterdam (ACTA), Vrije Universiteit Amsterdam, De Boelelaan 1117, 1081 HV, Amsterdam, the Netherlands
[d] Department of Oral Cell Biology, Academic Centre for Dentistry Amsterdam (ACTA), University of Amsterdam and Vrije Universiteit Amsterdam, Gustav Mahlerlaan 3004, 1081 LA, Amsterdam, the Netherlands

ARTICLE INFO

Keywords:
Bone tissue engineering
Finite element modeling
Fluid flow dynamics
Osteoblasts
Oxygen
Perfusion bioreactor
3D-printed scaffold

ABSTRACT

Fluid flow dynamics and oxygen-concentration in 3D-printed scaffolds within perfusion bioreactors are sensitive to controllable bioreactor parameters such as inlet flow rate. Here we aimed to determine fluid flow dynamics, oxygen-concentration, and cell proliferation and distribution in 3D-printed scaffolds as a result of different inlet flow rates of perfusion bioreactors using experiments and finite element modeling. Pre-osteoblasts were treated with 1 h pulsating fluid flow with low (0.8 Pa; PFF^{low}) or high peak shear stress (6.5 Pa; PFF^{high}), and nitric oxide (NO) production was measured to validate shear stress sensitivity. Computational analysis was performed to determine fluid flow between 3D-scaffold-strands at three inlet flow rates (0.02, 0.1, 0.5 ml/min) during 5 days. MC3T3-E1 pre-osteoblast proliferation, matrix production, and oxygen-consumption in response to fluid flow in 3D-printed scaffolds inside a perfusion bioreactor were experimentally assessed. PFF^{high} more strongly stimulated NO production by pre-osteoblasts than PFF^{low}. 3D-simulation demonstrated that dependent on inlet flow rate, fluid velocity reached a maximum (50–1200 μm/s) between scaffold-strands, and fluid shear stress (0.5–4 mPa) and wall shear stress (0.5–20 mPa) on scaffold-strands surfaces. At all inlet flow rates, gauge fluid pressure and oxygen-concentration were similar. The simulated cell proliferation and distribution, and oxygen-concentration data were in good agreement with the experimental results. In conclusion, varying a perfusion bioreactor's inlet flow rate locally affects fluid velocity, fluid shear stress, and wall shear stress inside 3D-printed scaffolds, but not gauge fluid pressure, and oxygen-concentration, which seems crucial for optimized bone tissue engineering strategies using bioreactors, scaffolds, and cells.

1. Introduction

The increasing demand for bone transplantation and limitations in autograft and allograft encourage the development of novel substrates for bone tissue engineering. In bone scaffold-based tissue engineering, fluid flow dynamics and oxygen concentration are pivotal parameters affecting cell proliferation, distribution, and activity within 3D-scaffolds. A major bottleneck in the 3D-bone tissue engineering field is the lack of efficient vascularization strategies, since a constant flow of

* Corresponding author. Department of Biomedical Engineering, Research Center for New Technologies in Life Science Engineering, University of Tehran, Tehran, P.O. Box 11365-4563, Iran.
E-mail addresses: seddiqi.hadi@gmail.com (H. Seddiqi), saatchi@ut.ac.ir (A. Saatchi), amoabediny@ut.ac.ir, amoabediny@ut.ac.ir (G. Amoabediny), m.helder@amsterdamumc.nl (M.N. Helder), so.abbasi1991@gmail.com (S. Abbasi Ravasjani), mrsafari1368@gmail.com (M. Safari Hajat Aghaei), j.jin@acta.nl (J. Jin), bzandiehdoulabi@acta.nl (B. Zandieh-Doulabi), j.kleinnulend@acta.nl (J. Klein-Nulend).
[1] Shared first authorship, H. Seddiqi and A. Saatchi contributed equally to this manuscript.
[2] Shared last authorship, B. Zandieh-Doulabi and J. Klein-Nulend contributed equally to this manuscript.

https://doi.org/10.1016/j.compbiomed.2020.103826
Received 20 February 2020; Received in revised form 15 May 2020; Accepted 15 May 2020
Available online 4 August 2020

List of abbreviations

DO	dissolved oxygen
NO	nitric oxide
PFF	pulsating fluid flow
3D	three-dimensional
WSS	wall shear stress

Glossary of Terms

u_i	$m.s^{-1}$ flow velocity component
x_i, x_j	spatial coordinates
η	Pa.s culture medium dynamic viscosity
ρ	$kg.m^{-3}$ density
p	Pa pressure
g	$m.s^{-2}$ acceleration of gravity
τ	Pa viscous stress tensor
c	$mol.m^{-3}$ dissolved oxygen concentration
D_c	$cm^2.s^{-1}$ diffusion coefficient
S_c	$mol.(m^3.s)^{-1}$ oxygen uptake rate of cells
μ_{max}	$1.s^{-1}$ maximum specific growth rate of cells
m_s	$mol.s^{-1}$ minimum oxygen consumption of cells
K_s	$mol.m^{-3}$ oxygen concentration at which oxygen consumption is half maximum
ρ_{cell}	(number of living cells).cm^{-2} cell density in the scaffold
Y_{XS}	$1.mol^{-1}$ yield of cells per unit oxygen
V_{max}	$mol.s^{-1}$ maximum oxygen consumption rate
$\boldsymbol{D_{cell}}$	$m^2.s^{-1}$ diffusivity of cell
μ_{cel}l	number of living cells.s^{-1} cell growth rate

oxygen and nutrients is needed to maintain viability and functionality of bone tissue constructs [1]. Flow culture causes homogeneous distribution of cells and matrix throughout the scaffold, while static culture results in a peripheral layer only [2]. Therefore, dynamic bioreactors are used to provide homogeneous bone tissue growth by facilitating nutrient transport and shear stress inside 3D-scaffolds [3,4]. These bioreactors enhance human mesenchymal stem cell (MSC) growth [5], osteogenic differentiation [6], mineralized matrix production [7], osteoblast cellularity and activity, and stimulate the formation of bone template in vitro [8,9]. Within a range of superficial flow velocities (80, 400, 800, 1, 200, and 1800 μm/s), corresponding to estimated initial shear stresses ranging from 0.6 to 20 mPa, flow velocities ranging from 400 to 800 μm/s yielded the best overall osteogenic responses [10]. Low perfusion flow rates (0.01–0.2 ml/min) increase osteoblast proliferation, while high rates (>1 ml/min) are associated with cell death throughout 3D-porous scaffolds [11]. Not only flow rate, but also pore size and porosity influence the bone formation process, i.e. minimum pore sizes required for 3D bone regeneration range from 100 μm to more than 400 μm [12,13]. Moreover, a pore size of ~100 μm is favored under hypoxic conditions to induce osteochondral bone formation, whereas a larger pore size of more than 300 μm directly initiates osteogenesis [14,15].

Mechanical forces play a major role in the regulation of bone remodeling in intact bone and bone repair [16]. Mechanical stimulation by *e.g.* fluid shear stress and fluid pressure modulates large-scale tissue-engineered bone formation [17,18]. Transmission of mechanical stress to bone cells occurs mainly via fluid shear stress [19]. Fluid shear stress increases nitric oxide (NO) synthesis by bone cells and osteogenically stimulated mesenchymal stem cells [20,21]. Therefore, increased NO production is a measure for their mechanosensitivity. Fluid shear stress ranging from 0.6 mPa to 20 mPa is beneficial for bone cell cultures [10]. Increasing fluid shear stress accelerates osteogenic differentiation of human bone marrow stromal cells and improves matrix mineralization, while mass transport inhibits the formation of mineralized matrix [22]. Fluid shear stress at 1200 mPa promotes terminal differentiation of MC3T3-E1 pre-osteoblasts [23]. Fluid shear stress at 1200 mPa also stimulates osteogenic differentiation of human periodontal ligament cells (hPDLCs) [24]. The relationship between mechanical loads and bone tissue differentiation is clear, but the local shear stress sensed by cells inside 3D-scaffolds is less clear. In addition, the effect of fluid pressure transients, which are necessary to drive the loading-induced fluid flow, on the regulation of bone remodeling in intact bone and bone repair is poorly understood. The mechanical stress state within 3D-scaffolds is further complicated when the pressure differential needed to drive fluid through the scaffold's channels is considered. Therefore, prediction of the fluid flow dynamics inside 3D-scaffolds is needed to better understand cell mechanotransduction in these systems.

Real time measurements on spatial properties in 3D bioreactor systems is very difficult. Measurement of the local velocity and shear stress fields is only possible at the scaffold outer walls using laser Doppler velocimetry [25,26] or particle image velocimetry [27], but this affects cell growth inside the 3D scaffolds. The mathematical modeling provides a basis for analyses of hydrodynamic shear stress and hydrodynamic pressure exerted directly by fluid flow acting on cells seeded within 3D-scaffolds [28,29]. The model can then produce detailed quantitative spatial and temporal knowledge of the fluid flow dynamics [30,31], oxygen transport [32], mechanical stimuli on cells, local stress distribution in the 3D scaffolds [33,34], and predict cell distribution and growth [35,36]. Mathematical modeling has been used to optimize and/or evaluate 3D scaffold designs in terms of oxygen transport, mechanical properties, and cell responses to external stimuli [37,38]. The level of insight offered by the modeling cannot be obtained by means of experiments alone.

In the present study, we first modulated fluid flow dynamics and oxygen concentration in a 3D-scaffold (0.1 cm diameter strands, total volume 216 mm^3) inside a perfusion bioreactor at three different inlet flow rates (0.02, 0.1, and 0.5 ml/min), corresponding to three different inlet flow velocities (0.01, 0.05, and 0.25 mm/s) during 5 days, by employing the finite element method as a computational fluid dynamics approach. Next, we experimentally validated that different fluid flow regimes differentially did affect the production of NO, which regulates canonical Wnt/β-catenin signaling by stimulation of osteogenesis [39]. Then poly(ε-caprolactone) (PCL) scaffolds were 3D-printed with a regular structure (diameter strands (mean ± SD), 0.075 ± 0.006 cm; total volume, 216 mm^3) by depositing the strands layer-by-layer with an alternating 0/90 lay-down pattern, and the surface of the scaffolds was modified by alkaline (NaOH) treatment. The seeding efficiency, as well as proliferation, matrix production, and oxygen consumption of MC3T3-E1 pre-osteoblasts in response to fluid flow in a 3D-printed scaffold inside a perfusion bioreactor was determined experimentally. This is the first study to evaluate, using finite element modeling combined with experimental validation, the precise influence of inlet flow rate on fluid velocity, fluid shear stress, wall shear stress (WSS), gauge fluid pressure, and oxygen concentration inside homogenous, cell-seeded 3D-printed scaffolds within perfusion bioreactors over time which may be pivotal for optimized bone tissue engineering.

2. Materials and methods

2.1. Computational fluid dynamics modeling

2.1.1. Model geometry

A 3D-scaffold with a regular internal structure measuring 0.6 × 0.6 × 0.6 cm (length × width × height; total volume, 216 × 10^{-3} cm^3; total

void volume, 131 cm^3), and a strand diameter of 0.1 cm inside a perfusion bioreactor was constructed in CAD software (COMSOL Multiphysics 5.2, Stockholm, Sweden) (Fig. 1(a)). The distance between the strands was 0.1 cm. Perfusion was initiated by allowing the inlet flow to enter directly at the top surface of the 3D-printed scaffold (Fig. 1(b)).

2.1.2. Model assumptions

To model the 3D-scaffold in the perfusion bioreactor, some assumptions were made about boundary conditions and initial conditions in order to simplify the mathematical modeling. The strands inside the scaffold and attached cell layers were assumed to be rigid and not affected by the fluid flow [40,41]. The strands topography variation was considered as negligible during the computational evaluation since collagenous matrix deposition, cell proliferation, and fluid flow on the strands did not change the strands topography significantly during the short time-span (5 days) of our study. The culture medium inside the scaffold was considered as incompressible, and homogeneous Newtonian fluid. The effect of heat dissipation from the culture medium was neglected. Therefore, the culture medium specifications, such as dynamic viscosity and density, were assumed to be constant during the computational analysis. It is assumed that the initial cell seeding was uniform throughout the 3D-scaffold. The cells were assumed to be attached to the outer surface of strands inside the scaffold during the simulation period. The thickness of the cell layers was assumed to be negligible compared to the diameter of the strands. Hence, it was assumed that the oxygen uptake rate of cells (equation (5)), and cell growth kinetics (equations (7) and (8)), occurred only on the outer surface of the strands. Also, the attached cell layers do not have any influence on the flow field. So, we neglect the effect of the attached cell layer on the fluid flow dynamics inside the scaffold. Oxygen supply, but not nutrients (*e.g.* glucose), was considered in this study.

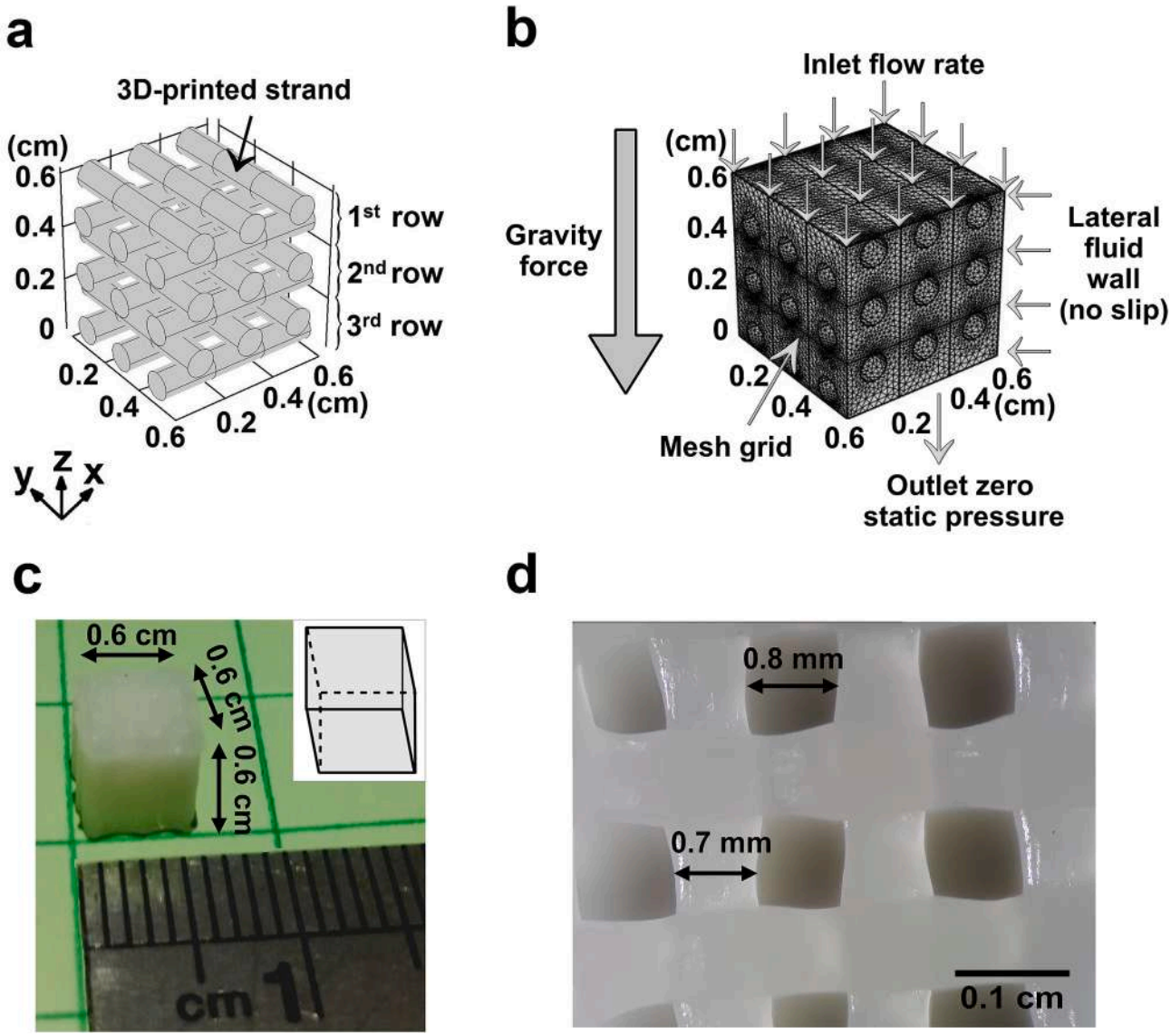

Fig. 1. Schematic illustration of a 3D-printed cubic scaffold measuring 0.6 × 0.6 × 0.6 cm (length × width × height; 100 μm diameter strands, total scaffold volume 216 mm^3) used to simulate fluid velocity, fluid shear stress, wall shear stress (WSS), fluid pressure, oxygen concentration, and cell density inside a perfusion bioreactor, as well as 3D-printed scaffold used in the experimental study. (a) Structure of the scaffold showing the outer surface of the strands inside the 3D-printed scaffold. (b) Simulation volume, mesh, and boundary conditions (inlet flow rate, outlet zero static pressure, no wall slip) applied in the numerical method. (c) Cubic 3D-printed scaffold (0.6 × 0.6 × 0.6 cm) used to determine the effect of fluid flow on MC3T3-E1 pre-osteoblast proliferation and distribution inside perfusion bioreactors. Also shown is a schematic of the scaffold. (d) Top view of the 3D-printed scaffold showing the internal structure (strands and voidage). The diameter of the strands was ~0.7 mm, and the void size of the scaffolds was ~0.8 mm.

2.1.3. Mathematical equations

To simulate the 3D-scaffold in the perfusion bioreactor, the fluid flow was modeled by laminar fluid flow equations (section 2.1.3.1) as described below. The oxygen concentration throughout the 3D-scaffold was modeled by using time-dependent convection-diffusion equations (section 2.1.3.2) during the modeling period (5 days), and the cell growth on the surface of the strands was modeled by using time-dependent cell proliferation and migration equations (section 2.1.3.3), as described below.

2.1.3.1. Laminar fluid flow. Navier-Stokes equation for incompressible fluid dynamics (momentum (equation (1)) and continuity (equation (2)) was used to model a fully developed and laminar flow [42].

$$\rho\frac{\partial \boldsymbol{u}}{\partial t}-\eta\nabla^2\boldsymbol{u}+\rho(\boldsymbol{u}.\nabla)\boldsymbol{u}+\nabla p=\boldsymbol{F} \tag{1}$$

$$\nabla.\boldsymbol{u}=0 \tag{2}$$

where **u**, ρ, η, and p are the fluid velocity field, fluid density, fluid dynamic viscosity, and fluid pressure respectively. Finally, **F** indicates hydrostatic pressure force, where $\mathbf{F}=\rho\mathbf{g}h$ (g is acceleration of gravity, and h is height of the scaffold) in the present study [42].

Solving the Navier-Stokes equation numerically yielded the fluid velocity field and fluid pressure. From the fluid velocity information, the fluid shear stress (τ) was attained by using the following constitutive relation for a Newtonian fluid:

$$\tau_{ij}=\mu\left(\frac{\partial \boldsymbol{U}_i}{\partial X_j}+\frac{\partial \boldsymbol{U}_j}{\partial X_i}\right) \tag{3}$$

2.1.3.2. Oxygen transport. Culture medium flows through the scaffold and transports nutrients and oxygen, which is essential for cells. The governing equation for single phase oxygen transfer through a scaffold is the convection–diffusion equation [43].

$$\frac{\partial \mathrm{C}}{\partial \mathrm{t}}=\nabla.(\mathrm{D}_c\nabla \mathrm{c})+\mathrm{S}_c-\mathbf{u}.\nabla \mathrm{c} \tag{4}$$

where *c* is the dissolved oxygen (DO) concentration in the fluid, D_c is diffusion coefficient. S_c is the oxygen uptake rate of cells described by modified Monod equation as follows [44–46]:

$$\mathrm{S}_c=\left(\frac{\mu_{\max}}{\mathrm{Y}_{\mathrm{XS}}}+\mathrm{m}_s\right)\rho_{cell}\frac{\mathrm{C}}{\mathrm{K}_s+\mathrm{C}} \tag{5}$$

where μ_{max} is maximum specific growth rate of cells, m_s is the minimum oxygen consumption by cells, K_s is the half-saturation constant of dissolved oxygen, defined as the dissolved oxygen concentration at which the consumption rate drops to half of its maximum value, ρ_{cell} is the cell density in the scaffold, and Y_{xs} is the yield of cells per unit oxygen which was described by the following equation [44]:

$$\mathrm{Y}_{\mathrm{XS}}=\frac{\mu_{\max}}{\mathrm{V}_{\max}-\mathrm{m}_s} \tag{6}$$

where V_{max} is maximum oxygen consumption rate.

2.1.3.3. Cell growth. Oxygen passing through the scaffold reaches the proliferating cells. Cell density variation in the scaffold depends on cell proliferation and migration [47,48], which were modeled by the following equation [44]:

$$\frac{\partial \rho_{cell}}{\partial t}=D_{cell}\nabla^2\rho_{cell}+\rho_{cell}\mu_{cell} \tag{7}$$

where D_{cell} is the cell diffusivity, and μ_{cell} is the cell growth rate, which was as follows [35,49]:

$$\mu_{cell}=\mathrm{Y}_{\mathrm{XS}}\left(\frac{\mathrm{S}_c}{\rho_{cell}}-\mathrm{m}_s\right) \tag{8}$$

The first-time derivative of cell density $\left(\frac{\partial \rho_{cell}}{\partial t}\right)$ was calculated first, and based on the value obtained we numerically calculated the cell density by equation [7].

2.1.4. Mesh generation

For the generation of finite element meshes, three physics-controlled meshes with coarse element size (total elements: 148592), normal element size (total elements: 323795), and fine element size (total elements: 522867) were constructed using COMSOL Multiphysics (v5.2, Stockholm, Sweden). The element type was tetrahedral, pyramid, and prism throughout the computational model. Tetrahedral elements were used since any 3D-geometry, regardless of shape or topology, can be meshed with tetrahedral elements. Furthermore, tetrahedral elements are the only kind of elements that can be used with adaptive mesh refinement, and therefore we preferred these elements for discretization of the 3D-domain in this study. We also used prism elements, since these elements have a high aspect ratio (longest edge-to-shortest edge ratio), which reduces the number of elements. We have used the prism elements where the FEM results of fluid dynamics, oxygen concentration, and cell density varied gradually in certain directions. Pyramid elements were used at the interfaces to connect the tetrahedral and prism elements wherever connection was needed. First-order, linear, finite element discretization was used for the laminar fluid flow and oxygen transport equations. Second order, quadratic, finite element discretization with Lagrange shape function was used for the cell growth equation. The maximum difference in the calculated average fluid velocity, fluid shear stress, oxygen concentration, and cell density between the mesh with normal element size and that with fine element size was ~5%, which was considered negligible. Therefore, the finite element mesh with normal element size (total elements:323795, tetrahedra, 247147; pyramids: 648; prisms: 76000) and 425169° of freedom was assumed to be fine enough to accurately determine the fluid velocity, fluid shear stress, wall shear stress, oxygen concentration, and cell proliferation and distribution inside the 3D-scaffold in a perfusion bioreactor. The average element quality was 0.66 measured by skewness, which is considered as good element quality for finite element modeling The maximum size of the mesh element was 0.318 mm, the minimum size of the mesh element was 0.06 mm, the maximum element growth rate was 1.13, the curvature factor was 0.5, and the resolution of the narrow area was 0.8 (Fig. 1 (b).

2.1.5. Initial and boundary conditions

Since partial differential equations were used, logical and sufficient initial and boundary conditions were needed. The initial fluid velocity was set to zero in the simulation volume. The oxygen concentration throughout the scaffold was initially set to a constant value (0.2×10^{-6} mol cm^{-3}), equal to the standard oxygen concentration in fresh medium [50]. The Initial cell density was based on the initial cell number seeded in the experimental part of our study. The detailed information of the model parameters and initial conditions used for modeling are presented in Table 1.

The fluid pressure at the outlet surface of the scaffold was set to zero as a boundary condition (Fig. 1(b)). No-slip boundary condition was applied to the inner surface of the scaffold (Fig. 1(b)). The hydrostatic pressure force was applied inside the scaffold volume against the z axis (Fig. 1(b)). As inlet flow boundary condition, constant inlet flow rates (0.02, 0.1, and 0.5 ml/min) were chosen based on those in peristaltic pumps (range 0.02–1 ml/min) generally used in experimental and simulation studies with perfusion bioreactors [11,51,52]. As inflow boundary condition, constant oxygen concentration was set to 0.2×10^{-6} mol cm^{-3}, equal to the oxygen concentration value in the culture

Table 1
Parameters and default values used in the simulation model.

Parameters	Expression	Value	References
C_0 (mol.cm^{-3})	Standard O_2 concentration in fresh medium	0.2×10^{-6}	[50]
$\rho_{initial}$ (cells.cm^{-2})	Initial cell density	3×10^4	
V_{max} (mol.(cell.s)$^{-1}$)	Maximum oxygen consumption rate	1.75×10^{-17}	[69]
K_s (mol.m^{-3})	Half velocity constant	0.01105	[70]
μ_{max} (s^{-1})	Maximum specific cell growth rate	5×10^{-6}	[70]
D_c (m^2.s^{-1})	Diffusion coefficient of oxygen	1×10^{-5}	[71,72]
D_{cell} (cm^2.s^{-1})	Cell motility coefficient	1×10^{-10}	[73]
T (°C)	Operational temperature	37	
ρ (kg.m^{-3})	Culture medium density	999.3	[50]
η (mPa.s)	Culture medium dynamic viscosity	0.69	[74]
P (atm)	Operation pressure	1	
G (m.s^{-2})	Acceleration of gravity	9.8	

medium reservoir.

2.1.6. Finite element modeling

The commercial finite element software package (COMSOL Multiphysics v5.2, Stockholm, Sweden) was used to assess the influence of the inlet flow rate of a perfusion bioreactor, as a controllable parameter, on fluid velocity, fluid shear stress, WSS, gauge fluid pressure, and cell density inside the 3D-printed scaffold with a regular internal structure and micro-dimension strands under perfusion conditions.

The finite element analysis used was Multiphysics coupling analysis. The finite element modeling was performed with time-dependent Fully Coupled solver. A MUltifrontal Massively Parallel Sparse (MUMPS) direct solver was used to evaluate the variables (fluid dynamics, oxygen concentration, and cell density) inside the 3D-scaffold in the bioreactor. The coupling of the convection-diffusion and fluid flow equations took place due to the dependency of the DO concentration (*c*; equation (4)) on the fluid velocity fields (u) inside the 3D-scaffold. Also, the coupling of the growth equations and convection-diffusion equations took place due to the dependency of the cell growth rate (μ_{cell}; equation (8)) on the DO fields (*c*; equation (4)) inside the 3D-scaffold.

2.1.7. Average fluid velocity, fluid shear stress, fluid pressure, WSS, oxygen concentration, and cell density calculation

The average values of fluid velocity, fluid shear stress, fluid pressure, WSS, oxygen concentration, and cell density were evaluated based on the following equation:

$$\theta_{ave} = \frac{\iiint \theta d\Omega}{\iiint d\Omega} \tag{9}$$

where θ is dependent variable (fluid velocity, fluid shear stress, fluid pressure, WSS, oxygen concentration, and cell density), and Ω is the spatial domain, that equals the void volume inside the 3D-scaffold for fluid velocity, fluid shear stress, fluid pressure, and oxygen concentration, and that equals the inner surface area of the 3D-scaffold for WSS and cell density.

2.2. Experimental method

2.2.1. Mechanical stimulation by pulsating fluid shear stress

To study the effects of fluid shear stress on MC3T3-E1 pre-osteoblasts in monolayer culture, two parallel plate flow chambers were used. Flow chamber dimensions: PFF^{high}, length: 7 cm, width: 2.4 cm, height: 0.03 cm; PFF^{low}, length: 2 cm, width: 1.4 cm, height: 0.02 cm. PFF^{high} (frequency: 1 Hz, peak shear stress: 6.5 Pa, pulse amplitude: 1 Pa, flow rate: 28.7 ml/min) and PFF^{low} (frequency: 1 Hz, peak shear stress: 0.8 Pa, pulse amplitude: 0.126 Pa, flow rate: 3.5 ml/min) was generated by pumping medium through a parallel-plate flow chamber containing MC3T3-E1 pre-osteoblasts (Fig. 2). α-Minimum Essential Medium (α-MEM; Life Technologies™, Waltham, MA, USA) with 5% platelet lysate, 100 U/ml penicillin (Sigma-Aldrich, Hamburg, Germany), 100 μg/ml streptomycin sulfate (Sigma-Aldrich), and 10 IU/ml heparin (LEO Pharma A/S, Ballerup, Denmark) to prevent coagulation, was driven into the chamber by hydrostatic pressure created by the vertical distance between a reservoir located above the chamber and a collecting reservoir located below the chamber, at 37 °C in a humidified atmosphere with 5% CO_2 in air. A pump refilled the top reservoir but did not affect the flow inside the chamber. Therefore, a constant level in the feeding reservoir was ensured by a refilling pump such that the flow rate in the parallel plate chamber was constant. Static cultures were kept in a Petri dish under similar conditions as the dynamic cultures. Medium samples of 500 μl were taken at 0, 10, 30, and 60 min of static culture, PFF^{high} and PFF^{low} treatment, and assayed for NO production.

2.2.2. Nitric oxide analysis

NO production was measured as nitrite (NO_2^-) accumulation in conditioned medium using Griess reagent containing 2% sulfanilamide, 0.2% naphtylethelene-diamine-dihydrochloride, and 5% H_3PO_4. Serial dilutions of 0.1 M $NaNO_2$ in α-MEM were used as a standard curve. The absorbance was measured at 540 nm with a Synergy HT® spectrophotometer.

2.2.3. 3D-printing of scaffolds

Scaffolds were printed by a 3DPLN2 bioprinter (3DPL, Tehran, Iran) using a thermo polymer extruder equipped with a needle with an inner diameter of 400 μm. Medical grade PCL (Mn 80,000 Da, density 1.145 g/ml; Sigma Aldrich, St. Louis, MO, USA) was melted at 75 °C in a heating tank. The PCL was extruded through a pre-heated needle at 0.4 MPa (4 Bar), and the PCL strands were plotted layer-by-layer with an alternating 0°/90° lay-down pattern. Seven cubic scaffolds measuring 0.6 × 0.6 × 0.6 cm (total volume 216×10^{-3} cm^3) were produced (Fig. 1(c)). The strand diameter was 0.075 ± 0.006 (mean ± SD) cm, and the void size inside the scaffolds 0.085 ± 0.007 cm (Fig. 1(d)). Mechanical properties of the 3D-printed scaffold have been described recently [15].

2.2.4. Chemical surface modification by introduction of carboxyl and hydroxyl groups

The 3D-printed scaffolds were submerged in 3 M NaOH solution (Merck, Darmstadt, Germany) for 24 h to produce carboxyl and hydroxyl groups on the surface, as this has been shown earlier to increase cell proliferation and matrix deposition [53]. Scaffolds were rinsed with deionized water until the pH of the rinsing water was neutral, air-dried, and UV sterilized for 30 min. They were immersed in 70% ethanol for 1 h prior to start of the experiments.

2.2.5. Cell culture and seeding onto the scaffolds

MC3T3-E1 pre-osteoblasts were obtained from the American Type Culture Collection (ATCC; Manassas, VA, USA). Cells were grown and maintained in α-Minimum Essential Medium (α-MEM; Gibco, Life 4 Technologies, Waltham, MA, USA) and supplemented with 10% fetal bovine serum (FBS; BioWest SAS, 5 Nuaille, France) in a humidified incubator with 5% CO_2 in air at 37 °C. After reaching ~75% confluency, cells were detached using 0.25% trypsin (Gibco, Invitrogen, Waltham, MA, USA) and 0.1% ethylenediaminetetraacetic acid (Merck, Darmstadt, Germany) in phosphate-buffered saline (PBS) at 37 °C. Cells were then re-suspended in α-MEM with 10% FBS and 1% PSF. The cell suspension was carefully distributed over the surface of 6 scaffolds at a concentration of 4.5×10^6 cells/cm^3 scaffold in 24-well culture plates. Cell attachment was allowed for 3 h, and 2 ml medium was added to cell/scaffold constructs. After one day incubation, three scaffolds were transferred to perfusion bioreactors and cultured for another 5 days. Then scaffolds were rinsed three times with PBS, fixed for 60 min with 4% paraformaldehyde at room temperature, and rinsed again with PBS.

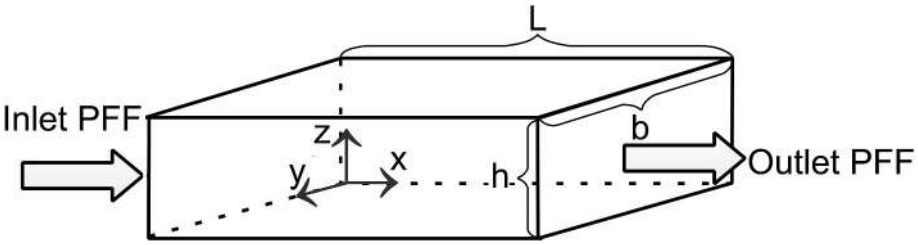

Fig. 2. Diagram of a parallel-plate flow chamber used to expose MC3T3-E1 osteoblasts to PFF. The chamber's width b, height h, and length L, are shown in x-y-z axes orientation. PFF was forced through the chamber by a steady pressure gradient along the x-axis. PFF is the abbreviation for pulsating fluid flow.

2.2.6. Perfusion bioreactor

Perfusion systems are designed to perfuse culture medium through the scaffold. The perfusion culture is used to increase the rates of mass transport through the interior of the scaffold compared with the rate of diffusion alone, and can be used to apply mechanical stimulation, in the form of shear stress, to cells in the scaffold, in order to achieve a desired cellular response. A perfusion bioreactor consisting of a close loop system with a reservoir and perfusion chamber was used. Culture medium flow was passed throughout the scaffold from top-to-bottom. A peristaltic pump (Ismatec REGLO ICC Digital Peristaltic Pump; 4-Channels, 12 Rollers) was used to obtain a 0.02 ml/min flow rate on the 3D-printed scaffolds. Medium reservoir volume was 70 ml at atmospheric pressure and 37 °C. For running the close loop setup, the cell-seeded scaffold was placed within a CO_2 incubator during culture.

2.2.7. Seeding efficiency

Four hours after cell seeding on the scaffold in a 24-well culture plate, cell/scaffold constructs were rinsed twice with PBS, and transferred to a new 6-well culture plate. Seeding efficiency was assessed by determining the number of cells attached to the wells of the 24-well culture plate as well as to the scaffolds, using AlamarBlue® fluorescent assay (Invitrogen, Frederick, MD, USA), according to the manufacturer's instructions. Cells attached to the culture plate and cell-scaffold constructs were incubated with 10% AlamarBlue® solution in fresh medium for 4 h in a humidified incubator with 5% CO_2 in air at 37 °C. Then the medium was harvested, and the fluorescence measured at 530–560 nm excitation and 590 nm emission with a Synergy HT® microplate reader (City, Country). Seeding efficiency was calculated according to the following equation:

$$\text{Seeding efficiency } (\%) = \frac{\text{number of cells attached to the scaffold}}{\text{number of cells attached to the scaffold} + \text{number of cells attached to the plate}} \times 100 \quad (10)$$

Three groups of the scaffolds seeding efficiency (54%) was measured 4 h after seeding. Scaffolds were assayed in triplicate.

2.2.8. Cell proliferation

Cell proliferation on scaffolds in perfusion bioreactors was assessed by dividing the total number of cells in the scaffolds after 5 days of culture by the number of cells in the scaffolds at day 0 as determined using the AlamarBlue® fluorescent assay as described under "seeding efficiency". We found a linear relationship between AlamarBlue® fluorescence and cell number (data not shown) [54]. After performing the AlamarBlue® assay at day 5, cell/scaffold constructs were fixed using 4% glutaraldehyde for further experiments. Per group three scaffolds were used.

2.2.9. Collagenous matrix deposition

Picrosirius red stain kit (Chondrex, Inc., Redmond, WA, USA) was used to visualize total collagen deposition, and to obtain an indication of cell distribution inside the scaffolds under dynamic and static condition at different layers of the scaffolds (top, middle, and bottom). After 5 days of culture, the cell/scaffold constructs were rinsed thoroughly with PBS, fixed in 4% formaldehyde, and stained for 2 h with picrosirius red at room temperature. Then, constructs were rinsed twice with acidified water (5 ml acetic acid/L distilled water), and visualized using a Nikon SMZ-10 stereo microscope (Nikon, Tokyo, Japan). Microscopic images were taken from top, middle, and bottom of the cell/scaffold constructs after dynamic or static culture.

2.2.10. Cell distribution

Nuclei of cells in of the scaffolds were fluorescently stained with DAPI (4′,6-diamidino-2-phenylindole, dihydrochloride; Thermo Fisher Scientific Inc. Bremen, Germany) solution (1 μg/ml) for 10 min. Fluorescent images were taken at random locations in sections (0.15*0.15 mm^2 section) of the cell/scaffold constructs after perfusion and static cultures using a fluorescence microscope. After staining, the sections were rinsed twice with PBS.

2.2.11. Oxygen concentration

To validate the simulated oxygen concentration inside a 3D-printed scaffold, a needle-type oxygen microsensor (PreSens, Regensburg, Germany) was used to measure the oxygen concentration daily in the inflow and outflow of a perfusion bioreactor during 5 days. For each measurement, a two-point calibration of the microsensor was performed. Ambient air (as 21% oxygen reference) and 100% CO_2 atmosphere (as 0% oxygen reference) were considered. The outflow oxygen concentration was normalized to fresh medium by the following equation to obtain the rate of oxygen consumption by MC3T3-E1 pre-osteoblasts during 5 days of dynamic culturing.

$$\text{Normalized outflow oxygen concentration} = \frac{\text{outflow oxygen concentration}}{\text{inflow oxygen concentraion}} \quad (11)$$

2.2.12. Statistical analysis

All experiments were carried out in triplicate. Data are presented as mean ± standard error of the mean (SEM), and were compared using *t*-test or two-way ANOVA. The *t*-test was used to test statistical significance of data on NO production by MC3T3-E1 pre-osteoblasts as a result of fluid flow treatment (Section 3.2.1), and two-way ANOVA for testing statistical significance of data on comparison of experimental and

Table 2
Numerical simulation of the effect of changes in inlet flow rate of a perfusion bioreactor containing a 3D-scaffold on average fluid velocity, average fluid shear stress, average wall shear stress (WSS), average fluid pressure, average oxygen concentration, and average cell density after 5 days. Increasing the inlet flow rate of perfusion bioreactor increased the average fluid velocity, average fluid shear stress, and average WSS. Average fluid pressure, average oxygen concentration, and average cell density inside the scaffold did not alter by changing the inlet flow rate of the perfusion bioreactor.

Simulation parameters	Inlet flow rate (ml/min)		
	0.02	0.1	0.5
Average fluid velocity (μm/s)	18	83	387
Average fluid shear stress (mPa)	0.09	0.38	1.69
Average WSS (mPa)	0.16	0.65	3.08
Average fluid pressure (Pa)	970	970	970
Average oxygen concentration (mol/m^3)	0.02	0.02	0.02
Average cell density ($cells/cm^2$)	5.65×10^4	5.65×10^4	5.65×10^4

WSS, wall shear stress.

simulation results (section 3.2.2). Differences were considered significant if $p < 0.05$.

3. Results

3.1. Numerical results

3.1.1. Average fluid pressure, average oxygen concentration, and average cell density inside a 3D-scaffold within a perfusion bioreactor

Average fluid velocity, average fluid shear stress, average WSS, average gauge fluid pressure, average oxygen concentration, and average cell density inside a 3D-scaffold within a perfusion bioreactor were related to the inlet flow rate (0.02, 0.1, and 0.5 ml/min) at 5 day (Table 2). By varying the perfusion bioreactor's inlet flow rate from 0.02 ml/min to 0.5 ml/min, the average fluid velocity, average fluid shear stress, and average WSS increased by 19 to 22-fold (Table 2). At all inlet flow rates, the average gauge fluid pressure, average oxygen concentration, and average cell density were similar at day 5 (Table 2).

3.1.2. Predicted inlet flow rate of a perfusion bioreactor containing a 3D-scaffold based on published WSS

Depending on the magnitude of the WSS, cell proliferation, mineralization, and/or differentiation may be enhanced. Based on the linear relationship between average WSS inside the scaffold within the perfusion bioreactor and inlet flow rate (inlet flow rate = 0.1619 × WSS), we predicted a range of inlet flow rates of a perfusion bioreactor containing a 3D-scaffold that would affect cell proliferation (3.2×10^{-4} - 6×10^{-2} ml/min), osteogenic differentiation (3.2×10^{-4} - 1.98×10^{2} ml/min), and/or mineralization (<4.9–49.5 ml/min) based on published WSS data using numerical methods (Table 3).

Future experimental studies on bone cell fate in a 3D-printed scaffold within a perfusion bioreactor could use FEM-predicted inlet flow rates to stimulate osteoblast proliferation, osteogenic differentiation, and/or mineralization.

Table 3
Predicted inlet flow rate of perfusion bioreactors containing a 3D-scaffold based on published WSS data on osteoblast cell proliferation, osteogenic differentiation, and/or mineralization using numerical methods.

Reference	Published WSS (mPa)	WSS effect on cells	Predicted inlet flow rate (ml/min)
[56]	0.002-0.4	↑Differentiation ↑Proliferation	3.2×10^{-4}-6×10^{-2}
[75]	30–300	↑Mineralization	$4.9–5 \times 10^{1}$
[76]	51	↑Mineralization	8.4
[60]	<30	↑Differentiation	<4.9
[22]	5–15	↑Differentiation ↑Mineralization	0.8-2.5
[24]	1200	↑Differentiation	1.98×10^{2}

WSS, wall shear stress; ↑ increase.

3.1.3. Fluid velocity and fluid shear stress distribution and magnitude inside a 3D-scaffold after 5 days

The fluid velocity and fluid shear stress in the void side of the 3D-scaffold corresponding to the different inlet flow rates (0.02, 0.1, and 0.5 ml/min) of a perfusion bioreactor were simulated, and illustrated along the zx plane (Fig. 3). The fluid velocity and fluid shear stress were symmetric around the zx plane (Fig. 3). As the inlet flow rate increased, the fluid velocity magnitude and fluid shear stress inside the scaffold increased as well (Fig. 3). The fluid velocity accelerated depending on the inlet flow rate (0.02 ml/min: 20–60 μm/s; 0.1 ml/min: 100–300 μm/s; 0.5 ml/min: 500–1500 μm/s) through the gap between two strands. The maximum fluid velocity also was dependent on the inlet flow rate (0.02 ml/min: 60 μm/s; 0.1 ml/min: 300 μm/s; 0.5 ml/min: 1500 μm/s) and was found between two strands in each layer. The magnitude of the fluid velocity was low (0.02 ml/min: < 20 μm/s; 0.1 ml/min: < 100 μm/s; 0.5 ml/min: < 500 μm/s) near the surface of the strands compared to other regions inside the scaffold. The perfusion flow resulting from different inlet flow rates produced different fluid shear stress on the strand surfaces (0.02 ml/min: > 0.5 mPa; 0.1 ml/min: > 1.5 mPa; 0.5 ml/min: > 8.0 mPa; Fig. 3). Spatial inhomogeneity and magnitude of the fluid velocity and fluid shear stress inside the scaffold increased by increasing the inlet flow rate of the perfusion bioreactor (Fig. 3).

3.1.4. WSS distribution and magnitude exerted on cells inside a 3D-scaffold during 5 days

The fluid velocity changes on the surface of the strands inside the 3D-printed scaffold resulted in the creation of WSS, which can be considered as the shear stress exerted on cells attached inside the scaffold. The effect of changes in inlet flow rate (0.02, 0.1, and 0.5 ml/min) of a perfusion bioreactor on WSS distribution and magnitude was simulated during 5 days (Fig. 4). WSS distribution on the strands surfaces was more homogeneous at 0.02 and 0.1 ml/min inlet flow rate than at 0.5 ml/min inlet flow rate. By increasing the inlet flow rate of the perfusion bioreactor, the WSS magnitude increased on all strands surfaces during 5 days (Fig. 4). At 0.02 ml/min inlet flow rate, WSS magnitude reached a maximum on the surface of the third row of strands inside the scaffold at 0.5 h, after which it declined until 5 days. At 0.1 ml/min inlet flow rate, WSS magnitude reached a maximum on the surface of the first and third rows of strands at 0.5 h, and declined on the third row of strands until 3 days. At 0.5 ml/min inlet flow rate, WSS magnitude reached a maximum on the surface of first and third rows of strands at 0.5 h, and declined on the third row of strands until 1 day (Fig. 4). At 0.02 and 0.1 ml/min inlet flow rates, WSS shear stress reached a steady state condition after 5 and 3 days respectively, while at 0.5 ml/min inlet flow rate, WSS already reached a steady state condition after 1 day due to the high inlet fluid velocity (200 μm/s) compared to that at 0.02 and 0.1 ml/min inlet flow rates (Fig. 4).

3.1.5. WSS distribution and magnitude inside a 3D-scaffold after 5 days

3D-view, side view, and top view of WSS distribution and magnitude as a result of varying inlet flow rate (0.02, 0.1, and 0.5 ml/min) of a perfusion bioreactor inside a 3D-scaffold at day 5 revealed that WSS distribution was more homogeneous at 0.02 ml/min than at 0.1 ml/min inlet flow rate (Fig. 5). It was also more homogeneous at 0.1 ml/min than at 0.5 ml/min inlet flow rate. WSS magnitude increased by enhancing the inlet flow rate (0.02 ml/min: 0.2 mPa, 0.1 ml/min: 1 mPa, 0.5 ml/min: 4 mPa). WSS magnitude on the surface of all strands where fluid was passing was higher than in other regions on the strands surfaces (Fig. 5).

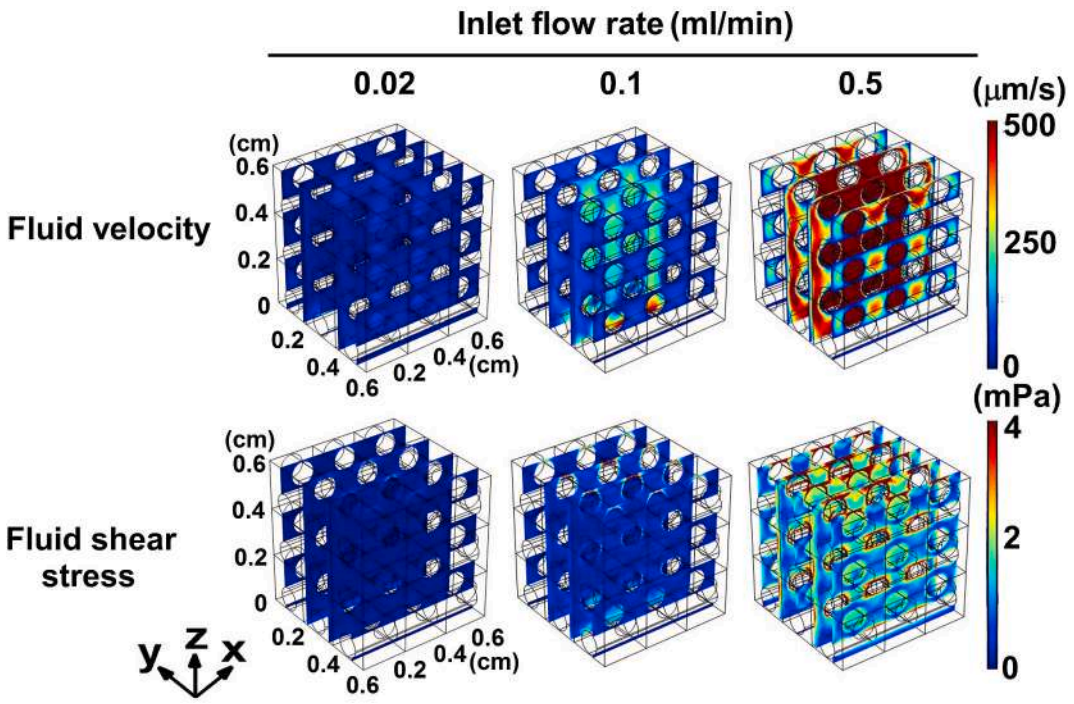

Fig. 3. Effect of changes in inlet flow rate (0.02, 01, 0.5 ml/min) of a perfusion bioreactor on the fluid velocity and fluid shear stress distribution and magnitude inside a 3D-scaffold after 5 days by using finite element modeling. Increasing the inlet flow rate enhanced fluid velocity and fluid shear stress distribution and magnitude inside the scaffold. The fluid velocity and fluid shear stress were in the void side of the 3D-scaffold.

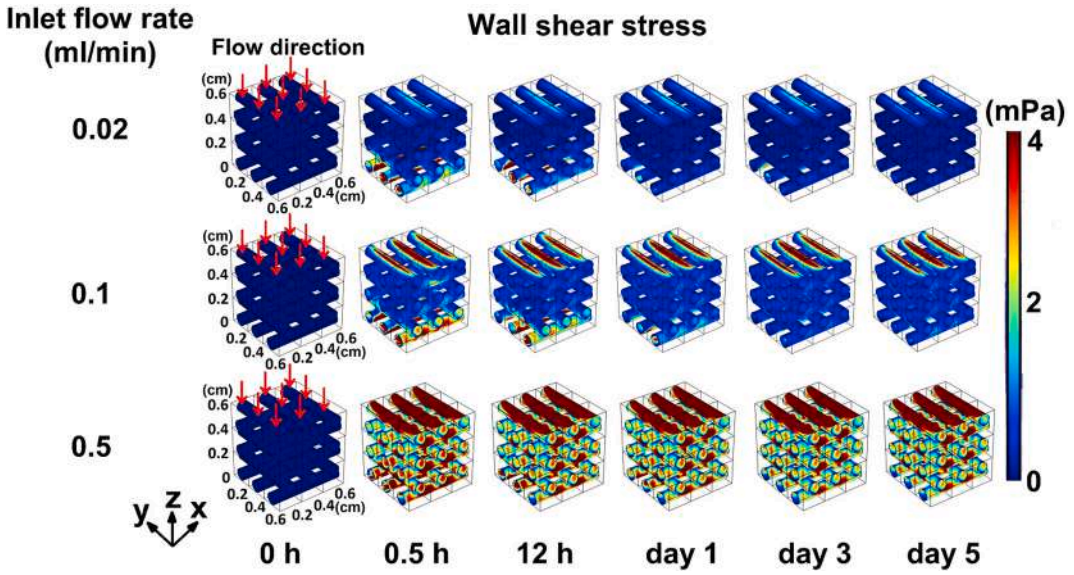

Fig. 4. Effect of changes in inlet flow rate (0.02, 01, 0.5 ml/min) of a perfusion bioreactor on wall shear stress (WSS) distribution and magnitude exerted on cells inside a 3D-printed scaffold during 5 days. Increasing the inlet flow rate enhanced WSS magnitude and distribution inside the scaffold at all time points measured. Red arrows, inlet flow direction. Black arrows, changes in WSS under inlet flow rate along with time. (For interpretation of the references to colour in this figure legend, the reader is referred to the Web version of this article.)

3.1.6. WSS distribution and magnitude exerted on cells attached to each row of strands inside a 3D-scaffold during 5 days

The effect of changes in inlet flow rate (0.02, 0.1, and 0.5 ml/min) of a perfusion bioreactor on the discrete probability distribution of the WSS magnitude on each row of the strands inside the scaffold during 5 days was calculated (Fig. 6). At each row of the strands, WSS magnitude of a maximum relative area (i.e. the area with a specific WSS magnitude divided by the total area inside the scaffold) was different at different inlet flow rates. WSS magnitude inside the scaffold increased by enhancing the inlet flow rate at all time points. At all inlet flow rates, the WSS distribution and magnitude at the first and second row of strands was similar at all time points, while they decreased over 5 days at the third row of strands (Fig. 6). At 0.02 and 0.1 ml/min inlet flow rates, maximum relative area was found on the surface of the third row of strands inside the scaffold (0.02 ml/min: 16%; 0.1 ml/min: 32%) at 0.5 h, while at 0.5 ml/min inlet flow rate, it was found on the first and third rows of strands (~12%), resulting in different relative areas with a broad range of WSS magnitude (0–20 mPa). At the first row of strands, the WSS

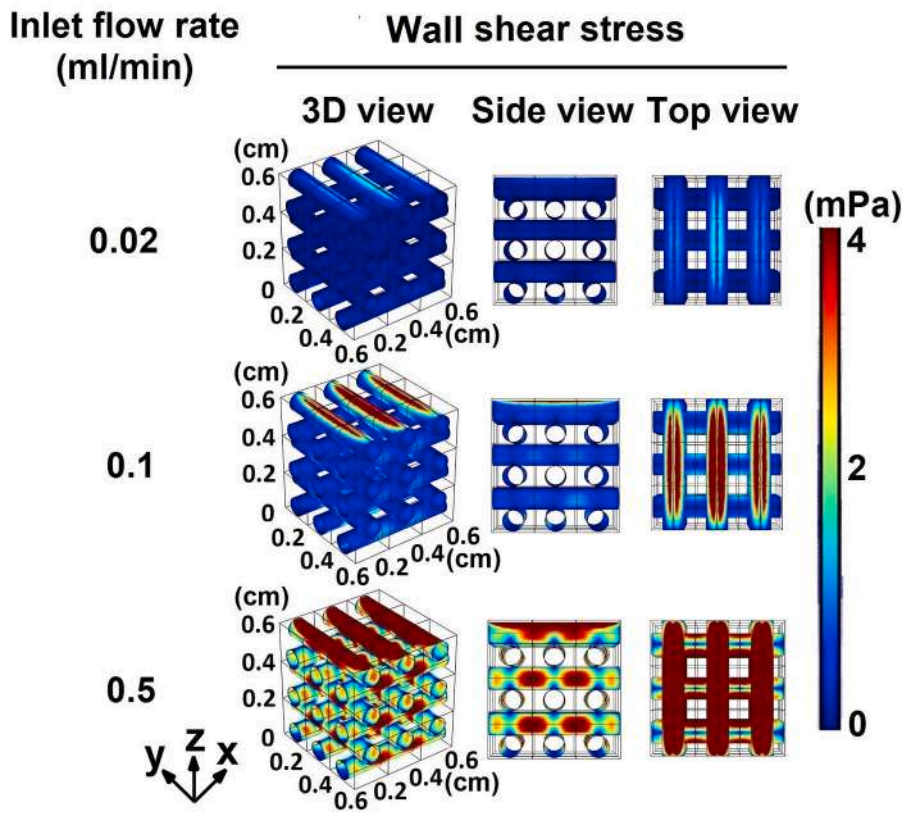

Fig. 5. 3D view, side view, and top view of wall shear stress (WSS) distribution and magnitude as a result of varying inlet flow rate (0.02, 0.1, and 0.5 ml/min) of a perfusion bioreactor inside a 3D-printed scaffold after 5 days. WSS distribution and magnitude inside the scaffold varied according to the magnitude of the inlet flow rate. 3D view: WSS was inhomogeneous at higher inlet flow rates. Side view: WSS was highest on the surface of all strands where the fluid was passing. Top view: WSS magnitude on the surface of the strands increased by increasing the inlet flow rate.

variation at 0.02 ml/min inlet flow rate was less (0–2 mPa) than at 0.1 ml/min inlet flow rate (0–10 mPa) and at 0.5 ml/min inlet flow rate (0–20 mPa) at all time points measured (Fig. 6). At the second row of strands, the WSS variation at 0.02 ml/min inlet flow rate was less (0–1 mPa) than at 0.1 ml/min inlet flow rate (0–2 mPa) and at 0.5 ml/min inlet flow rate (0–7 mPa) at all time points measured (Fig. 6). At the third row of strands, WSS variation (0–5 mPa) at 0.02 ml/min inlet flow rate was less than at 0.1 ml/min inlet flow rate (0–10 mPa) and at 0.5 ml/min inlet flow rate (0–20 mPa; Fig. 6).

3.1.7. Average WSS distribution and magnitude on each row of strands inside a 3D-scaffold during 5 days

The average WSS on the different rows of strands increased by enhancing the inlet flow rate (Fig. 7). At the first row of the strands, the average WSS increased 6.3-fold by increasing the inlet flow rate from 0.02 to 0.1 ml/min, and 3.9-fold by increasing the inlet flow rate from 0.1 to 0.5 ml/min after 5 days (Fig. 7). At the second row of strands, the average WSS increased 4.8-fold by increasing the inlet flow rate from 0.02 to 0.1 ml/min, and 4.9-fold by increasing the inlet flow rate from 0.1 to 0.5 ml/min. At the third row of strands, the average WSS increased 2.9-fold by increasing the inlet flow rate from 0.02 to 0.1 ml/min, and 4.1-fold by increasing the inlet flow rate from 0.1 to 0.5 ml/min after 5 days (Fig. 7).

3.1.8. Cell density and its first-time derivative inside a 3D-scaffold during 5 days

To investigate the effect of inlet flow rate (0.02, 0.1, and 0.5 ml/min) of a perfusion bioreactor on cell proliferation and cell proliferation rate inside the 3D-scaffold, cell density and first-time derivative of cell density inside the scaffold were simulated (Fig. 8). At all inlet flow rates after 5 days, the cell density inside the scaffold was ~1.9-fold higher than the initial cell density (Fig. 8(a)), and first time-derivative of cell density increased from 0 to ~0.8 cells/(cm^2.s) (Fig. 8(b)).

3.1.9. Gauge fluid pressure, oxygen concentration, and cell density inside a 3D-scaffold after 5 days

At all inlet flow rates, the gauge fluid pressure increased (from 0 to 60 mPa) uniformly from the top to the bottom row of strands inside the scaffold, while the oxygen concentration and cell density were similar throughout the scaffold after 5 days (Fig. 9). The gauge fluid pressure magnitude increased by 10 Pa between each row of strands from top to bottom due to hydrostatic pressure force. Oxygen concentration and cell density were similar throughout the scaffold (Fig. 9).

3.2. Experimental results

3.2.1. Effect of fluid flow on NO production by MC3T3-E1 pre-osteoblasts

Mechanical loading by PFF^{high}, but not PFF^{low}, rapidly (within 10 min) enhanced NO production by MC3T3-E1 osteoblasts (Fig. 10(a)). Both PFF^{high} and PFF^{low} stimulated NO production at later time points. PFF^{high} increased NO production after 10 min by 72-fold, at 30 min by 22-fold, and at 60 min by 13-fold compared to static control conditions (Fig. 10(a)). PFF^{Low} did not affect NO production at 10 min, but increased NO production after 30 min by 10-fold, and at 60 min by 8-fold compared to static control conditions (Fig. 10(b)). Thus, PFF^{high} more strongly affected NO production at all time points measured compared to PFF^{low} (Fig. 10(b)).

3.2.2. MC3T3-E1 pre-osteoblast proliferation, distribution, and collagenous matrix deposition, as well as oxygen concentration inside 3D-printed scaffolds after 5 days of culture

To validate cell proliferation and distribution, as well as oxygen concentration inside a 3D-printed scaffold in a perfusion bioreactor, MC3T3-E1 pre-osteoblast proliferation and distribution, matrix production, and oxygen consumption inside the scaffold to a 0.02 ml/min fluid flow rate in a perfusion bioreactor was investigated. Cells cultured inside a 3D-printed scaffold in a perfusion bioreactor deposited visibly more collagenous matrix throughout the scaffolds compared to cells in

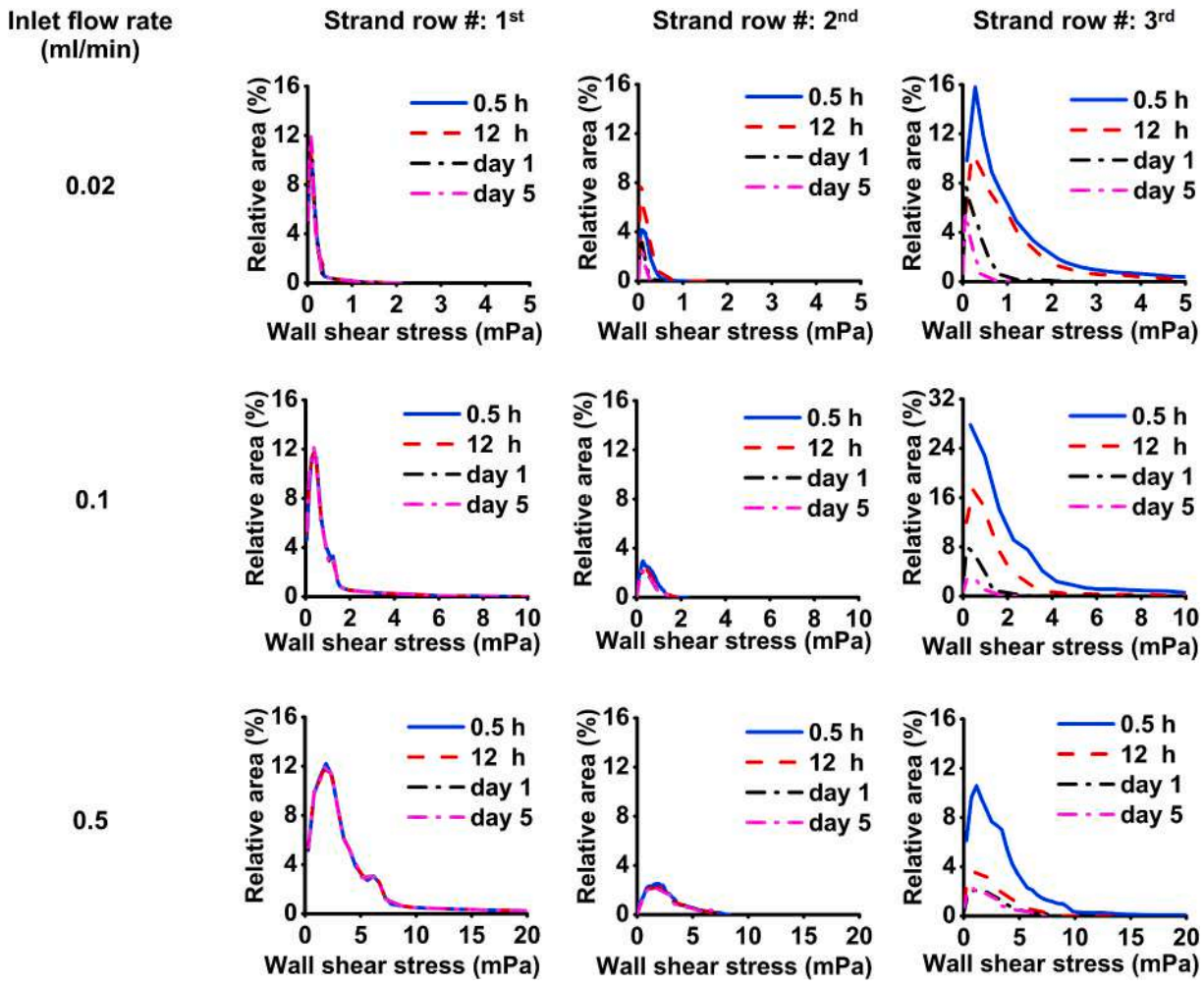

Fig. 6. Effect of changes in inlet flow rate (0.02, 0.1, 0.5 ml/min) of a perfusion bioreactor on wall shear stress (WSS) distribution and magnitude exerted on cells attached to each row of strands inside a 3D-printed scaffold during 5 days. The inlet flow rate affected the WSS distribution and magnitude on each row of strands inside the scaffold. Relative area: the area with a specific WSS divided by the total area inside the 3D-printed scaffold. Note the different scales of the x- and y-axes.

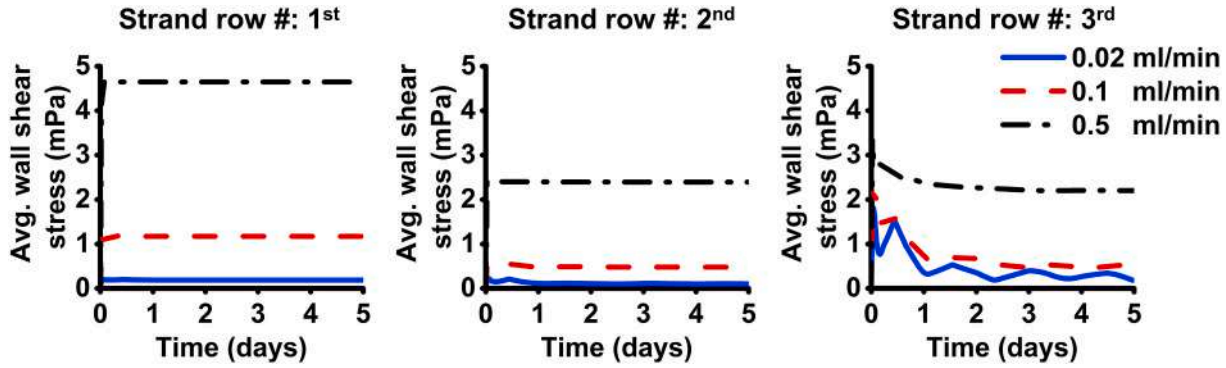

Fig. 7. Effect of changes in inlet flow rate (0.02, 01, 0.5 ml/min) of a perfusion bioreactor on average wall shear stress (WSS) distribution and magnitude on each row of strands inside a 3D-printed scaffold during 5 days. The inlet flow rate affected the average WSS magnitude on each row of strands. Increasing the inlet flow rate enhanced average fluid shear stress on each row of strands.

static culture (Fig. 11 (a)). Total collagen deposition was visualized experimentally to obtain an indication of cell distribution inside the scaffolds under dynamic and static condition at different layers of the scaffolds (top, middle, and bottom). Collagenous matrix deposition was more homogenous on the scaffold in a perfusion bioreactor compared to static culture after 5 days of culture (Fig. 11 (a)). MC3T3-E1 pre-osteoblast distribution inside a scaffold in a perfusion bioreactor was more homogeneous compared to static culture. Cell proliferation inside 3D-printed scaffolds in a perfusion bioreactor was measured experimentally after 5 days of culture and compared relative to day 0, and these results were compared with the simulation results during 5 days (Fig. 11 (b)). The simulated cell proliferation was derived from the cell density in the 3D-scaffold at different time points. The simulated cell proliferation data were in good agreement with the experimental results during 5

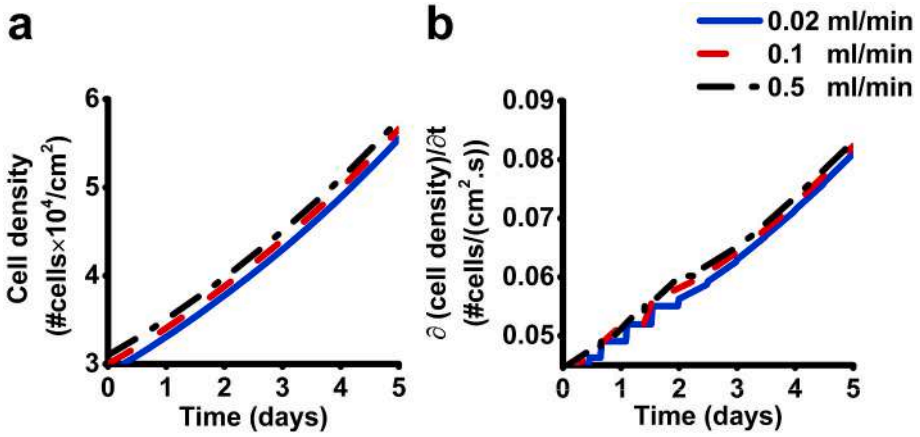

Fig. 8. Effect of changes in inlet flow rate (0.02, 0.1, and 0.5 ml/min) of a perfusion bioreactor on the cell density and first-time derivative of cell density inside a 3D-printed scaffold during 5 days. The inlet flow rate did not affect the magnitude and distribution of the cell density and its first-time derivative on each row of strands. (a) Cell density, and (b) First-time derivative of cell density increased at all inlet flow rates similarly during 5 days.

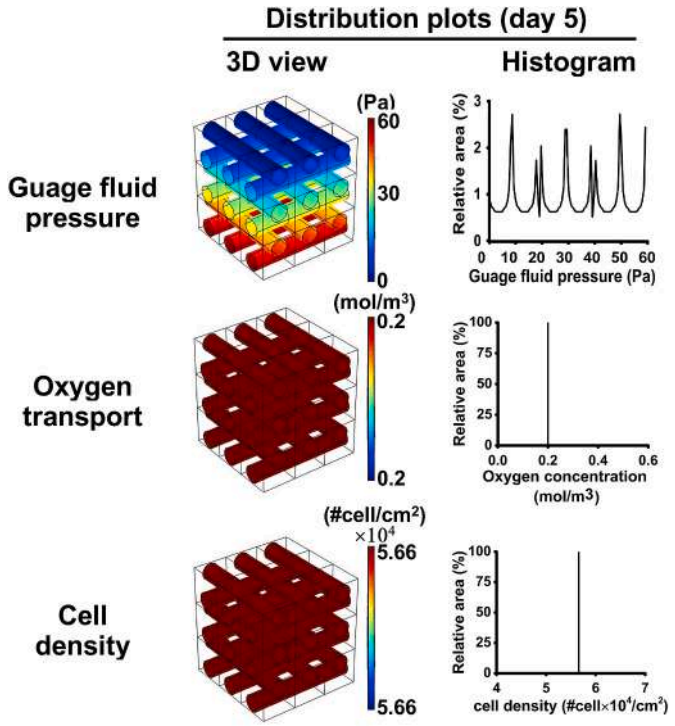

Fig. 9. 3D-view and histogram of distribution and magnitude of gauge fluid pressure, oxygen concentration, and cell density inside a 3D-printed scaffold in a perfusion bioreactor after 5 days. 3D-view: gauge fluid pressure increased uniformly from the top row to the bottom row of strands inside the scaffold. Distribution of oxygen concentration and cell density is homogeneous throughout the scaffold after 5 days. Histogram: gauge fluid pressure on the strands surface was inhomogeneous. Gauge fluid pressure peaked at each row of strands. Oxygen concentration and cell density were constant throughout the scaffold.

days of culture in a perfusion bioreactor (Fig. 11 (b)). The simulation results for cell proliferation were not significantly different from experimental results at day 5 (Fig. 11 (c)). Using fluorescent images of nuclei, cell distribution in the scaffold was more homogenous inside perfusion bioreactor compared to static culture (Fig. 11 (d)). Normalized outflow oxygen concentration consumed by cells inside the scaffolds was measured to validate the oxygen profile inside the scaffold. The normalized outflow oxygen concentrations were similar during 5 days, which was in good agreement with the simulated oxygen concentrations under dynamic condition inside the perfusion bioreactor (Fig. 11 (e)).

4. Discussion

Mathematical modeling coupled with experiments can be employed in the optimization process to develop bioreactor designs [38]. Here detailed information is provided about fluid flow dynamics, oxygen transfer, and cell proliferation and distribution within homogenous 3D-printed scaffolds inside perfusion bioreactors at different inlet flow rates using finite element modeling and experiments in which an inlet flow rate of 0.02 ml/min was used. The inlet flow rate of a perfusion bioreactor, as a controllable parameter, did affect the magnitude and distribution of fluid velocity, fluid shear stress, and WSS throughout the scaffold, while gauge fluid pressure, oxygen concentration, and cell density were constant throughout the scaffold. By increasing the inlet flow rate of the perfusion bioreactor, the magnitude and distribution of fluid velocity, fluid shear stress, and WSS inside the scaffold increased. The average fluid velocity, average fluid shear stress, and average WSS inside the scaffold within the perfusion bioreactor increased almost linearly with the inlet flow rate. The average shear stress in 3D scaffolds has been shown to be directly proportional to the inflow velocity of perfusion bioreactor by mathematical modeling [28,29]. Average gauge fluid pressure, average oxygen concentration, and average cell density was similar at all inlet flow rates of the perfusion bioreactor. Variation in the controllable parameters (inlet flow rate) might help to guide future scaffold design as well as experimental bone tissue engineering studies.

WSS affects cell behavior inside 3D scaffolds within perfusion bioreactors [55]. The effect of inlet flow rate of the perfusion bioreactor on the WSS inside the 3D-scaffold was estimated according to the relationship among the inlet flow rate and fluid velocity. Depending on the magnitude of the WSS, cell proliferation [56], mineralization [57], and/or differentiation [6] may be enhanced. Unfortunately, this cannot be predicted by the currently existing mathematical models. Our simulation model showed that the inner surface of the scaffold was exposed to different WSS magnitudes, which were found within the entire scaffold. High WSS occurred on the strands surface, which resulted from a no-slip boundary condition on the strands surface and the fluid velocity gradient. The WSS magnitude and distribution increased by enhancing the inlet flow rate of the perfusion bioreactor. Computational fluid dynamics models have predicted that a WSS of 0.1–10 mPa inside scaffolds is favorable for bone cell differentiation [58,59], and a WSS <30 mPa correlates with enhanced osteoblast differentiation [60]. We found that the WSS on the 3D-printed strands surfaces was <10 mPa at all inlet flow rates modeled, which falls in the range of published WSS of 0–10 mPa

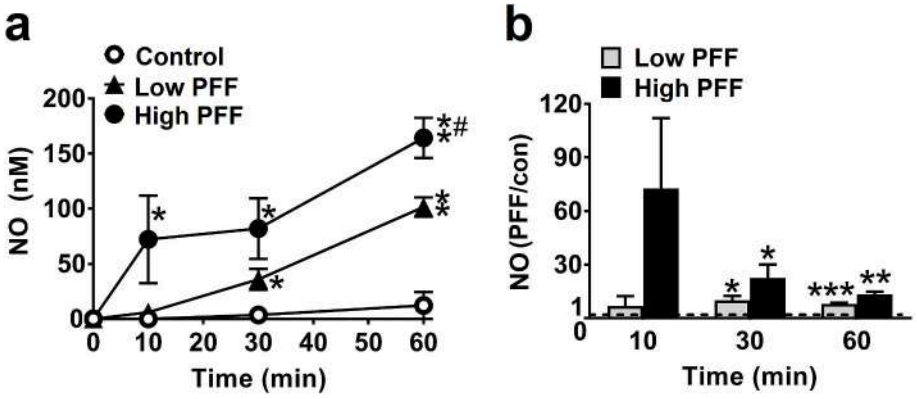

Fig. 10. Effect of 1 h PFF with low peak shear stress (PFF^{low}, 0.8 Pa) or high peak shear stress (PFF^{high}, 6.5 Pa) on NO production by MC3T3-E1 osteoblasts. (a) PFF^{high}, but not PFF^{low}, rapidly, within 10 min, increased NO production. Both PFF^{high} and PFF^{low} stimulated NO production at later time points. Values are mean ± SEM, n = 3–5. (b) PFF^{high} more strongly affected NO production than PFF^{low}. Values are mean ± SEM of PFF-over-static control ratios (PFF/static, n = 3–5), dashed line, PFF/static = 1 (no effect). *Significantly different from static control, $p < 0.05$, **$p < 0.005$, ***$p < 0.0005$. #Significantly different from PFF^{low}, $p < 0.05$. NO, nitric oxide; PFF, pulsating fluid flow.

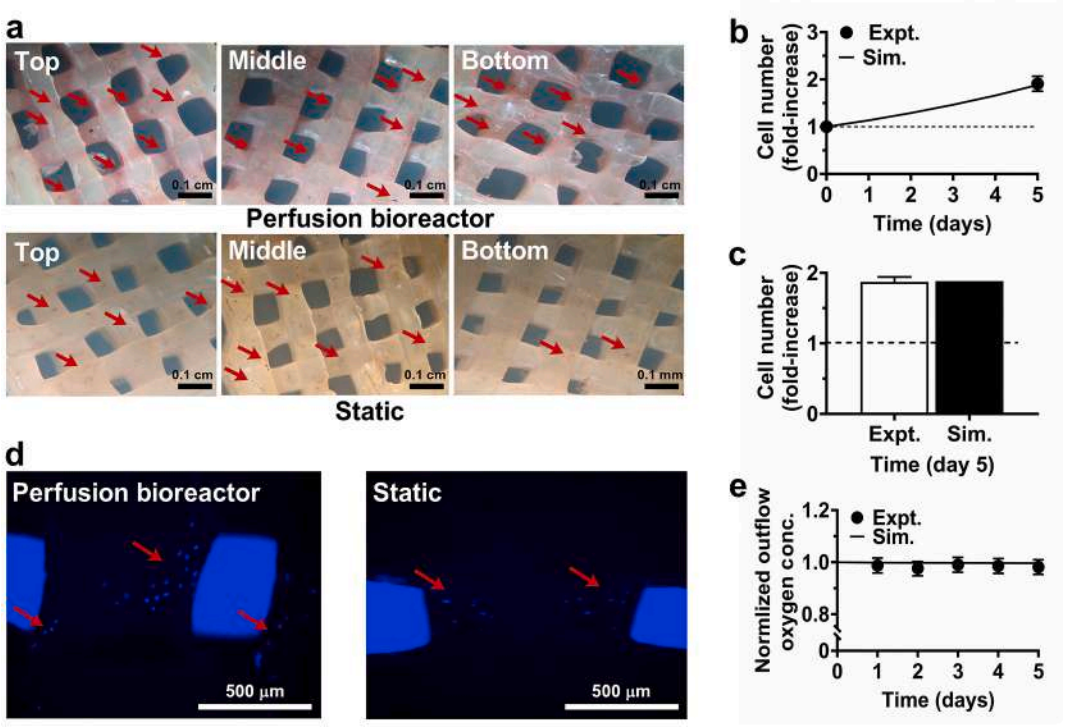

Fig. 11. MC3T3-E1 preosteoblast proliferation and collagenous matrix deposition, as well as normalized outflow oxygen concentration inside a 3D-printed scaffold in a perfusion bioreactor after 5 days of culture to experimentally validate the simulation results. (a) Collagenous matrix deposition by MC3T3-E1 preosteoblasts cultured on strands inside 3D-printed scaffolds in a perfusion bioreactor and static condition. More collagen (red) was observed on the strands surface inside scaffolds cultured in a perfusion bioreactor compared to static condition. Moreover, collagenous matrix deposition was more homogenous on a scaffold in a perfusion bioreactor compared to static condition. Scale bar, 0.1 cm. Red arrows, collagen. (b) Cell proliferation inside 3D scaffolds was measured experimentally after 5 days of culture in a perfusion bioreactor and compared with simulation results during 5 days. Cell proliferation inside the scaffolds was compared relative to day 0. The experimental results and simulation results were in good agreement at all time points measured. (c) MC3T3-E1 pre-osteoblast proliferation on scaffolds in perfusion bioreactor was measured experimentally as well as computationally. Cell proliferation on scaffolds was compared relative to day 0. The simulated results of cell proliferation were in good agreement with the experimental results at day 5 of culture in perfusion bioreactor. (d) Fluorescent images of DAPI-stained nuclei of cells cultured in perfusion bioreactor and static condition to exhibit cell distribution. Cell distribution was more homogenous on scaffold in perfusion bioreactor compared to static condition. Scale bar, 500 μm. Red arrows, cell nuclei. (e) Comparison between experimental and simulation results of normalized outflow oxygen concentration in a 3D-printed scaffold cultured inside a perfusion bioreactor during 5 days. Normalized oxygen concentration inside scaffolds was measured during 5 days of culture and compared with simulation results. The calculated oxygen concentrations inside the scaffolds were in good agreement with the measured concentrations in the scaffolds inside the perfusion bioreactor. (For interpretation of the references to colour in this figure legend, the reader is referred to the Web version of this article.)

and WSS<30 mPa enhancing osteoblast differentiation [60], which might suggest osteoblast differentiation inside our 3D-scaffold. A WSS magnitude of 5–15 mPa inside a scaffold could accelerate osteogenic differentiation and increase mineralization of MSCs [18]. We found that the surface area inside the 3D-printed scaffold with 0.5 ml/min inlet flow rate of the perfusion bioreactor experienced a WSS of 0–20 mPa, suggesting enhanced osteogenic differentiation potential of MSCs inside the scaffold. Moreover, a fluid shear stress of 0.002–0.4 mPa increases osteoblast proliferation and differentiation [56]. We found that the WSS was <0.1 mPa in the scaffold with 0.02 ml/min inlet flow rate of the perfusion bioreactor, suggesting enhanced proliferation and osteogenic differentiation of MSCs inside the scaffold. For all inlet flow rates, we

found that the WSS on the surface of the third row of the strands varied during 5 days. Thus, cells attached to this row of strands are exposed to variations in shear stress over time, which affects their behavior.

Our findings indicated that the perfusion bioreactor provided a strong flow without reverse flow within the 3D-printed scaffold in the perfusion bioreactor. The fluid velocity changed based on the available fluid surface within the scaffold. Therefore, when the fluid entered the scaffold and reached the first row of strands, the fluid velocity magnitude significantly increased at all inlet flow rates. Since liquid has the tendency to flow in the median available scaffold fields, the fluid velocity increased the void between the strands inside the scaffold. The variation of the fluid velocity enhanced near the strands surfaces. Therefore, maximum fluid shear stress occurred on the strands surfaces. The 3D-printed interconnectivity allowed the fluid flow to reach all internal scaffold walls, as well as a constant oxygen concentration through the whole inner surface of the scaffold. Thus, cell distribution was homogenous on the strands surface inside the scaffold. The interconnected pore network structure of the 3D-printed scaffold allows oxygen transfer into the cells attached to the strands of the scaffold. We measured cell proliferation throughout the scaffold, thus also in the center of the scaffold. The cells did climb into the center of the scaffold as demonstrated by extensive collagen production, which was more pronounced in the perfusion bioreactor compared to the static control.

Bone tissue engineering is currently limited by the inability to adequately vascularize tissues in vitro or in vivo which limits cell survival inside 3D scaffolds [61]. Bone graft survival requires rapid and sufficient vascularization. Oxygen diffusion and transport limitations are still a challenge in bone tissue engineering [62]. The oxygen concentration significantly decreases in the center of 3D-porous scaffolds independent of whether or not the medium flow is forced through the scaffold [63]. Therefore, cultured 3D-porous scaffolds are associated with oxygen gradients, which might result in inhomogeneous tissue quality [64]. Since oxygen diffusion is limited to only 200 μm from a blood vessel, cells lying beyond this physiological border suffer from hypoxia [65]. Under hypoxia, MSCs fail to survive, since they are unable to adapt their glucose consumption and do not possess the necessary glycolytic reserves to maintain their metabolism for more than three days [66]. Perfusion bioreactors are used to prevent cell death, but they do not entirely eliminate 3D-porous scaffold-associated oxygen gradients [67,68]. On the other hand, we found that the oxygen concentration and distribution were constant inside the 3D-printed scaffold in the perfusion bioreactor during 5 days, using experiments and finite element modeling. Although oxygen was consumed by cells in the scaffold, the oxygen concentration throughout the scaffold did not change during 5 days of culture, since the perfused fluid flow provided sufficient oxygen for consumption. The inlet flow rate of the perfusion bioreactor ensured a homogeneous oxygen supply in the scaffold, thus allowing the oxygen concentration to be controlled inside our 3D-printed scaffold. Therefore, 3D-printed scaffolds with rapid internal vascularization are an ideal bone substitute to provide sufficient oxygen and to overcome hypoxia inside 3D-constructs in perfusion bioreactors.

In the top and bottom region of the scaffold, cell density and growth rate seemed similar at all inlet flow rates of the bioreactor. This may be explained by the fact that cells at the bottom surface of the scaffold were provided with fluid that had previously perfused to the top surface of the scaffold. This fluid might contain as many nutrients as the fluid at the top layer of the scaffold. Although increased inlet flow rate of a perfusion bioreactor improves oxygen supply to the central scaffold regions, unfavorable cell detachment as a result of excessive shear stress does occur [8]. This warrants the evaluation of the optimal fluid flow rate for each individual cell–scaffold–bioreactor setup.

Mathematical modeling can predict cell distribution and growth in 3D-scaffolds in static and dynamic cultures of bone tissue [35,36], but still mathematical has limitations. One major limitation of the model presented was a lack of a mathematical equation to assess the effect of fluid dynamics on osteoblast behavior (proliferation, differentiation, mineralization, *etc*), since this is currently not possible with the existing modeling methods available. In addition, after cell proliferation, cells will start to produce extracellular matrix during culture. The support structure will become filled with extracellular matrix resulting in a geometrical change of the 3D-printed scaffolds. Inhomogeneous matrix deposition and cell distribution will eventually change flow patterns. However, since matrix deposition and cell proliferation did not change significantly, we have considered this negligible during the short time-span (5 days) of our study. Another limitation of our study was that the irregularity of the 3D-printed scaffold might influence the results. However, we considered the irregularity as negligible based on the low standard deviation of the diameter of the strands (mean ± SD), 0.075 ± 0.006 cm and the void size inside the scaffolds (mean ± SD), 0.085 ± 0.007 cm. We speculate that the effect of irregularity on the results would be negligible/small.

We conclude that a major issue inside the 3D-printed scaffold is fluid flow dynamics, which is controllable by inlet flow rate of perfusion bioreactor, whereas oxygen concentration and cell proliferation appear to be a minor important issue. Our findings provide a quantitative insight into the fluid flow dynamics, oxygen concentration, and cell proliferation and distribution within a 3D-printed scaffold containing cells in a perfusion bioreactor, which will have important implications for bone tissue engineering strategies using bioreactors, scaffolds, and cells.

5. Conclusions

We conclude that the inlet flow rate of the bioreactor, as a controllable parameter, significantly affects the magnitude and distribution of fluid velocity, fluid shear stress, and wall shear stress inside the 3D-printed scaffold, while gauge fluid pressure, oxygen concentration, and cells were homogeneously distributed inside the scaffold during 5 days. Therefore, a major issue inside the 3D-printed scaffold is fluid flow dynamics, which is controllable by inlet flow rate of perfusion bioreactor, whereas oxygen concentration and cell proliferation appear to be a minor important issue. By increasing the inlet flow rate of a perfusion bioreactor, the magnitude and distribution of fluid velocity, fluid shear stress, and wall shear stress inside the scaffold increased. The results of this study reveal information about the selection of the bioreactor inlet flow rate for optimal cell culture in bone tissue engineering. Our findings provide a quantitative insight into the fluid flow dynamics, oxygen transport, and cell proliferation and distribution within a 3D-printed scaffold containing cells in a perfusion bioreactor, which will have important implications for bone tissue engineering strategies using bioreactors, scaffolds, and cells.

6. Summary

In bone scaffold-based tissue engineering, fluid flow dynamics and oxygen concentration are pivotal parameters affecting cell proliferation, distribution, and activity within 3D-scaffolds. Fluid flow dynamics and oxygen concentration in 3D-printed scaffolds within perfusion bioreactors are sensitive to controllable bioreactor parameters such as inlet flow rate. Unfortunately, due to the complicated microstructure of the 3D-printed scaffolds, it is not possible to perform experimental analysis on fluid flow dynamics and oxygen concentration distribution within 3D-printed scaffolds. Moreover, mathematical modeling and simulation of bone tissue-engineering systems are helpful in this sense. In this study, we aimed to determine the distribution of fluid flow dynamics, oxygen concentration, and cell density in 3D-printed scaffolds as a result of different inlet flow rates of perfusion bioreactors using finite element modeling. Osteoblasts were treated with 1 h pulsating fluid flow with low (0.8 Pa; PFF^{low}) or high peak shear stress (6.5 Pa; PFF^{high}), and nitric oxide (NO) production was measured to validate shear stress sensitivity. Computational analysis was performed to determine fluid flow between 3D-printed scaffold-strands at three inlet flow rates (0.02, 0.1, 0.5 ml/

min) during 5 days. PFF^{high} more strongly stimulated NO production by osteoblasts than PFF^{low}. 3D-simulation indicated that the perfusion bioreactor provided a strong flow without reverse flow within the 3D-printed scaffold in the perfusion bioreactor. The 3D-printed interconnectivity allowed the fluid flow to reach all internal scaffold walls, as well as a constant oxygen concentration through the whole inner surface of the scaffold. The interconnected pore network structure of the 3D-printed scaffold allows oxygen transfer into the cells attached to the strands of the scaffold. 3D-simulation also demonstrated that dependent on inlet flow rate, fluid velocity reached a maximum (50–1200 μm/s) between scaffold strands, and fluid shear stress (0.5–4 mPa) and wall shear stress (0.5–20 mPa) on scaffold strands surfaces. At all inlet flow rates, gauge fluid pressure and oxygen concentration were similar. In conclusion, varying a perfusion bioreactor's inlet flow rate, as a controllable parameter, locally affects the magnitude and distribution of fluid velocity, fluid shear stress, and wall shear stress inside 3D-printed scaffolds, but not gauge fluid pressure, and oxygen concentration, which seems crucial for optimized bone tissue engineering strategies using bioreactors, scaffolds, and cells. Therefore, a major issue inside 3D-printed scaffolds inside perfusion bioreactors is fluid flow dynamics, which is controllable by inlet flow rate, whereas oxygen concentration and cell proliferation appear to be an issue of minor importance. The results of this study reveal information about the selection of the bioreactor inlet flow rate for optimal cell culture in bone tissue engineering. Our study helps to increase the knowledge of the fluid flow dynamics and oxygen transport in 3D-printed scaffolds in perfusion bioreactors.

Declaration of competing interest

All authors declare that they have no competing of interest.

Acknowledgements

The work of J. Jin was granted by the China Scholarship Council (CSC, No. 201608530156). The authors are thankful to the High Performance Computing Research Center at Amirkabir University of Technology, Tehran, Iran, for providing computational facilities.

References

[1] W. Zhang Yin, Z. Zhang, X. Jiang, Recent advances in scaffold design and material for vascularized tissue-engineered bone regeneration, Adv. Healthcare Mater. 8 (2019) 1801433, https://doi.org/10.1002/adhm.201801433.
[2] D. Mitra, J. Whitehead, O.W. Yasui, J.K. Leach, Bioreactor culture duration of engineered constructs influences bone formation by mesenchymal stem cells, Biomaterials 146 (2017) 29–39, https://doi.org/10.1016/j.biomaterials.2017.08.044.
[3] G. Bouet, M. Cruel, C. Laurent, L. Vico, L. Malaval, D. Marchat, Validation of an in vitro 3D bone culture model with perfused and mechanically stressed ceramic scaffold, Eur. Cell. Mater. 29 (2015) 250–267, https://doi.org/10.22203/ecm.v029a19.
[4] P.S. Lee, H. Eckert, R. Hess, M. Gelinsky, D. Rancourt, R. Krawetz, G. Cuniberti, D. Scharnweber, Developing a customized perfusion bioreactor prototype with controlled positional variability in oxygen partial pressure for bone and cartilage tissue engineering, Tissue Eng. C Methods 23 (2017) 286–297, https://doi.org/10.1089/ten.tec.2016.0244.
[5] Y.A. Petrenko, A.Y. Petrenko, I. Martin, D. Wendt, Perfusion bioreactor-based cryopreservation of 3D human mesenchymal stromal cell tissue grafts, Cryobiology 76 (2017) 150–153, https://doi.org/10.1016/j.cryobiol.2017.04.001.
[6] J.R. Vetsch, D.C. Betts, R. Muller, S. Hofmann, Flow velocity-driven differentiation of human mesenchymal stromal cells in silk fibroin scaffolds: a combined experimental and computational approach, PloS One 12 (2017), https://doi.org/10.1371/journal.pone.0180781 e0180781.
[7] C. Liu, R. Abedian, R. Meister, C. Haasper, C. Hurschler, C. Krettek, G. von Lewinski, M. Jagodzinski, Influence of perfusion and compression on the proliferation and differentiation of bone mesenchymal stromal cells seeded on polyurethane scaffolds, Biomaterials 33 (2012) 1052–1064, https://doi.org/10.1016/j.biomaterials.2011.10.041.
[8] J.C. Bernhard, E. Hulphers, B. Rieder, J. Ferguson, D. Runzler, T. Nau, H. Redi, G. Vunjak-Novakovic, Perfusion enhances hypertrophic chondrocyte matrix deposition, but not the bone formation, Tissue Eng. 24 (2018) 1022–1033, https://doi.org/10.1089/ten.tea.2017.0356.
[9] S. Bhumiratana, J.C. Bernhard, D.M. Alfi, K. Yeager, R.E. Eton, J. Bova, F. Shah, J. M. Gimble, M.J. Lopez, S.B. Eisig, G. Vunjak-Novakovic, Tissue-engineered autologous grafts for facial bone reconstruction, Sci. Transl. Med. 8 (2016) 343ra83, https://doi.org/10.1126/scitranslmed.aad5904.
[10] W.L. Grayson, D. Marolt, S. Bhumiratana, M. Frohlich, X.E. Guo, G. Vunjak-Novakovic, Optimizing the medium perfusion rate in bone tissue engineering bioreactors, Biotechnol. Bioeng. 108 (2011) 1159–1170, https://doi.org/10.1002/bit.23024.
[11] S.H. Cartmell, B.D. Porter, A.J. García, R.E. Guldberg, Effects of medium perfusion rate on cell-seeded three-dimensional bone constructs in vitro, Tissue Eng. 9 (2003) 1197–1203, https://doi.org/10.1089/10763270360728107.
[12] I. Bruzauskaite, D. Bironaite, E. Bagdonas, E. Bernotiene, Scaffolds and cells for tissue regeneration: different scaffold pore sizes-different cell effects, Cytotechnology 68 (2016) 355–369, https://doi.org/10.1007/s10616-015-9895-4.
[13] F. Zhao, T.J. Vaughan, L.M. McNamara, Quantification of fluid shear stress in bone tissue engineering scaffolds with spherical and cubical pore architectures, Biomech. Model. Mechanobiol. 15 (2016) 561–577, https://doi.org/10.1007/s10237-015-0710-0.
[14] V. Karageorgiou, D. Kaplan, Porosity of 3D biomaterial scaffolds and osteogenesis, Biomaterials (26) (2005), https://doi.org/10.1016/j.biomaterials.2005.02.002, 5474-91.
[15] Y. Zamani, G. Amoabediny, J. Mohammadi, H. Seddiqi, M.N. Helder, B. Zandieh-Doulabi, J. Klein-Nulend, J.H. Koolstra, 3D-printed poly (Ɛ-caprolactone) scaffold with gradient mechanical properties according to force distribution in the mandible for mandibular bone tissue engineering, J. Mech. Behav. Biomed. 104 (2020) 103638, https://doi.org/10.1016/j.jmbbm.2020.103638.
[16] M. Mullender, A. El Haj, Y. Yang, M. Van Duin, E. Burger, J. Klein-Nulend, Mechanotransduction of bone cells in vitro: mechanobiology of bone tissue, Med. Biol. Eng. Comput. 42 (2004) 14–21, https://doi.org/10.1002/term.1942.
[17] C. Wittkowske, G.C. Reilly, D. Lacroix, C.M. Perrault, In vitro bone cell models: impact of fluid shear stress on bone formation, Front. Bioeng. Biotechnol. 4 (2016) 87, https://doi.org/10.3389/fbioe.2016.00087.
[18] E. Stavenschi, M.A. Corrigan, G.P. Johnson, M. Riffault, D.A. Hoey, Physiological cyclic hydrostatic pressure induces osteogenic lineage commitment of human bone marrow stem cells: a systematic study, Stem Cell Res. Ther. 9 (2018) 276, https://doi.org/10.1186/s13287-018-1025-8.
[19] E.H. Burger, J. Klein-Nulend, Mechanotransduction in bone–role of the lacuno-canalicular network, Faseb. J. 13 (Suppl) (1999) S101–S112, https://doi.org/10.1096/fasebj.13.9001.s101.
[20] J. Klein-Nulend, C.M. Semeins, N.E. Ajubi, P.J. Nijweide, E.H. Burger, Pulsating fluid flow increases nitric oxide (NO) synthesis by osteocytes but not periosteal fibroblasts - correlation with prostaglandin upregulation, Biochem. Biophys. Res. Commun. 217 (1995) 640–648, https://doi.org/10.1006/bbrc.1995.2822.
[21] G.S. Tjabringa, P.S. Vezeridis, B. Zandieh-Doulabi, M.N. Helder, P.I.J.M. Wuisman, J. Klein-Nulend, Polyamines modulate nitric oxide production and COX-2 gene expression in response to mechanical loading in human adipose tissue-derived mesenchymal stem cells, Stem Cell. 24 (2006) 2262–2269, https://doi.org/10.1634/stemcells.2005-0625.
[22] D. Li, T. Tang, J. Lu, K. Dai, Effects of flow shear stress and mass transport on the construction of a large-scale tissue-engineered bone in a perfusion bioreactor, Tissue Eng. 15 (2009) 2773–2783, https://doi.org/10.1089/ten.tea.2008.0540.
[23] Z.H. Mai, Z.L. Peng, J.L. Zhang, L. Chen, H.Y. Liang, C.A.I. Bin, A.I. Hong, miRNA expression profile during fluid shear stress-induced osteogenic differentiation in MC3T3-E1 cells, Chinese Med J 126 (2013) 1544–1550.
[24] M. Tang, Z. Peng, Z. Mai, L. Chen, Q. Mao, Z. Chen, Q. Chen, L. Liu, Y. Wang, H. Ai, Fluid shear stress stimulates osteogenic differentiation of human periodontal ligament cells via the extracellular signal-regulated kinase 1/2 and p38 mitogen-activated protein kinase signaling pathways, J. Periodontol. 85 (2014) 1806–1813, https://doi.org/10.1902/jop.2014.140244.
[25] D.I. Hollnagel, P.E. Summers, D. Poulikakos, S.S. Kollias, Comparative velocity investigations in cerebral arteries and aneurysms: 3D phase-contrast MR angiography, laser Doppler velocimetry and computational fluid dynamics, NMR Biomed. 22 (2009) 795–808, https://doi.org/10.1002/nbm.1389.
[26] C.H. Yap, N. Saikrishnan, A.P. Yoganathan, Experimental measurement of dynamic fluid shear stress on the ventricular surface of the aortic valve leaflet, Biomech. Model. Mechanobiol. 11 (2012) 231–244, https://doi.org/10.1007/s10237-011-0306-2.
[27] C. Roloff, P. Berg, T. Redel, G. Janiga, D. Thévenin, Tomographic particle image velocimetry for the validation of hemodynamic simulations in an intracranial aneurysm, Conf. Proc. IEEE Eng. Med. Biol. Soc. (2017) 1340–1343, https://doi.org/10.1109/embc.2017.8037080, 2017.
[28] C. Sandino, J. Planell, D. Lacroix, A finite element study of mechanical stimuli in scaffolds for bone tissue engineering, J. Biomech. 41 (2008) 1005–1014, https://doi.org/10.1016/j.jbiomech.2007.12.011.
[29] A. Lesman, Y. Blinder, S. Levenberg, Modeling of flow-induced shear stress applied on 3D cellular scaffolds: implications for vascular tissue engineering, Biotechnol. Bioeng. 105 (2010) 645–654, https://doi.org/10.1002/bit.22555.
[30] J.R. Vetsch, R. Müller, S. Hofmann, The evolution of simulation techniques for dynamic bone tissue engineering in bioreactors, J. Tissue Eng. Regen. Med. 9 (2015) 903–917, https://doi.org/10.1002/term.1733.
[31] L. Liu, Q. Shi, Q. Chen, Z. Li, Mathematical modeling of bone in-growth into undegradable porous periodic scaffolds under mechanical stimulus, J. Tissue Eng. 10 (2019), https://doi.org/10.1177/2041731419827167, 2041731419827167.
[32] M. Cioffi, J. Küffer, S. Ströbel, G. Dubini, I. Martin, D. Wendt, Computational evaluation of oxygen and shear stress distributions in 3D perfusion culture systems:

macro-scale and micro-structured models, J. Biomech. 41 (2008) 2918–2925, https://doi.org/10.1016/j.jbiomech.2008.07.023.
[33] E. Askari, I. Cengiz, J. Alves, B. Henriques, P. Flores, M. Fredel, R.L. Reis, J. M. Oliveira, F.S. Silva, J. Mesquita-Guimarães, Micro-CT based finite element modelling and experimental characterization of the compressive mechanical properties of 3-D zirconia scaffolds for bone tissue engineering, J. Mech. Behav. Biomed. Mater. 102 (2020) 103516, https://doi.org/10.1016/j.jmbbm.2019.103516.
[34] A. Saatchi, H. Seddiqi, G. Amoabediny, M.N. Helder, B. Zandieh-Doulabi, J. Klein-Nulend, Computational fluid dynamics in 3D-printed scaffolds with different strand-orientation in perfusion bioreactors. Iran, J. Chem. Chem. Eng. (2019). In press.
[35] F. Mokhtari-Jafari, G. Amoabediny, N. Haghighipour, R. Zarghami, A. Saatchi, J. Akbari, N. Salehi-Nik, Mathematical modeling of cell growth in a 3D scaffold and validation of static and dynamic cultures, Eng. Life Sci. 16 (2016) 290–298, https://doi.org/10.1002/elsc.201500047.
[36] E. Magrofuoco, M. Flaibani, M. Giomo, N. Elvassore, Cell culture distribution in a three-dimensional porous scaffold in perfusion bioreactor, Biochem. Eng. J. 146 (2019) 10–19, https://doi.org/10.1016/j.bej.2019.02.023.
[37] J.M. Pedersen, Y.-S. Shim, V. Hans, M.B. Phillips, J.M. Macdonald, G. Walker, E. M. Andersen, H.J. Clewell, M. Yoon, Fluid dynamic modeling to support the development of flow-based hepatocyte culture systems for metabolism studies, Front. Bioeng. Biotechnol. 4 (2016) 72, https://doi.org/10.3389/fbioe.2016.00072.
[38] C.W. Kang, Y. Wang, M. Tania, H. Zhou, Y. Gao, T. Ba, G.D. Sean Tan, S. Kim, H. L. Leo, Computational fluid modeling and performance analysis of a bidirectional rotating perfusion culture system, Biotechnol. Prog. 29 (2013) 1002–1012, https://doi.org/10.1002/btpr.1736.
[39] N. Bandara, S. Gurusinghe, S.Y. Lim, H. Chen, S. Chen, D. Wang, B. Hilbert, L. X. Wang, P. Strappe, Molecular control of nitric oxide synthesis through eNOS and caveolin-1 interaction regulates osteogenic differentiation of adipose-derived stem cells by modulation of Wnt/β-catenin signaling, Stem Cell Res. Ther. 7 (2016) 182, https://doi.org/10.1186/s13287-016-0442-9.
[40] R. Voronov, S. VanGordon, V.I. Sikavitsas, D.V. Papavassiliou, Computational modeling of flow-induced shear stresses within 3D salt-leached porous scaffolds imaged via micro-CT, J. Biomech. 43 (2010) 1279–1286. https://doi: 10.1016/j.jbiomech.2010.01.007.
[41] M.S. Hossain, D. Bergstrom, X. Chen, Modelling and simulation of the chondrocyte cell growth, glucose consumption and lactate production within a porous tissue scaffold inside a perfusion bioreactor, Biotechnol. Rep. 5 (2015) 55–62. https://doi: 10.1016/j.btre.2014.12.002.
[42] P. Vossenberg, G.A. Higuera, G. van Straten, C.A. van Blitterswijk, A.J. van Boxtel, Darcian permeability constant as indicator for shear stresses in regular scaffold systems for tissue engineering, Biomech. Model. Mechanobiol. 8 (2009) 499–507, https://doi.org/10.1007/s10237-009-0153-6.
[43] J.S. Soares, M.S. Sacks, A triphasic constrained mixture model of engineered tissue formation under in vitro dynamic mechanical conditioning, Biomech. Model. Mechanobiol. 15 (2016) 293–316, https://doi.org/10.1007/s10237-015-0687-8.
[44] T.I. Croll, S. Gentz, K. Mueller, M. Davidson, A.J. O'Connor, G.W. Stevens, J. J. Cooper-White, Modelling oxygen diffusion and cell growth in a porous, vascularising scaffold for soft tissue engineering applications, Chem. Eng. Sci. 60 (2005) 4924–4934, https://doi.org/10.1016/j.ces.2005.03.051.
[45] C.D. de Gooijer, R.H. Wijffels, J. Tramper, Growth and substrate consumption of Nitrobacter agilis cells immobilized in carrageenan: part 1. Dynamic modeling, Biotechnol. Bioeng. 38 (1991) 224–231, https://doi.org/10.1002/bit.260380303.
[46] R.H. Wijffels, C.D. de Gooijer, S. Kortekaas, J. Tramper, Growth and substrate consumption of Nitrobacter agilis cells immobilized in carrageenan: part 2. Model evaluation, Biotechnol. Bioeng. 38 (1991) 232–240, https://doi.org/10.1002/bit.260380304.
[47] S. Galarza, H. Kim, N. Atay, S.R. Peyton, J.M. Munson, 2D or 3D? How cell motility measurements are conserved across dimensions in vitro and translate in vivo, Bioeng. Transl. Med. 5 (2020), https://doi.org/10.1101/627281 e10148.
[48] C.M. Franz, G.E. Jones, A.J. Ridley, Cell migration in development and disease, Dev. Cell 2 (2002) 153–158, https://doi.org/10.1016/s1534-5807(02)00120-x.
[49] K. Han, O. Levenspiel, Extended Monod kinetics for substrate, product, and cell inhibition, Biotechnol. Bioeng. 32 (1988) 430–447, https://doi.org/10.1002/bit.260320404.
[50] F. Coletti, S. Macchietto, N. Elvassore, Mathematical modeling of three-dimensional cell cultures in perfusion bioreactors, Ind. Eng. Chem. Res. 45 (2006) 8158–8169, https://doi.org/10.1021/ie051144v.
[51] R.J. McCoy, C. Jungreuthmayer, F.J. O'Brien, Influence of flow rate and scaffold pore size on cell behavior during mechanical stimulation in a flow perfusion bioreactor, Biotechnol. Bioeng. 109 (2012) 1583–1594, https://doi.org/10.1002/bit.24424.
[52] F. Maes, T. Claessens, M. Moesen, H. Van Oosterwyck, P. Van Ransbeeck, P. Verdonck, Computational models for wall shear stress estimation in scaffolds: a comparative study of two complete geometries, J. Biomech. 45 (2012) 1586–1592, https://doi.org/10.1016/j.jbiomech.2012.04.015.
[53] Y. Zamani, J. Mohammadi, G. Amoabediny, D.O. Visscher, M.N. Helder, B. Zandieh-Doulabi, J. Klein-Nulend, Enhanced osteogenic activity by MC3T3-E1 pre-osteoblasts on chemically surface-modified poly (ε-caprolactone) 3D-printed scaffolds compared to RGD immobilized scaffolds, Biomed. Mater. 14 (2018), https://doi.org/10.1088/1748-605x/aaeb82, 015008.
[54] F.A.S. van Esterik, B. Zandieh-Doulabi, C.J. Kleverlaan, J. Klein-Nulend, Enhanced osteogenic and vasculogenic differentiation potential of human adipose stem cells on biphasic calcium phosphate scaffolds in fibrin gels, Stem Cell. Int. 2016 (2016) 1–12, https://doi.org/10.1155/2016/1934270.
[55] G. Chen, R. Xu, C. Zhang, Y. Lv, Responses of MSCs to 3D scaffold matrix mechanical properties under oscillatory perfusion culture, ACS Appl. Mater. Interfaces 9 (2017) 1207–1218, https://doi.org/10.1021/acsami.6b10745.
[56] W. Yu, H. Qu, G. Hu, Q. Zhang, K. Song, H. Guan, T. Liu, J. Qin, A microfluidic-based multi-shear device for investigating the effects of low fluid-induced stresses on osteoblasts, PloS One 9 (2014), https://doi.org/10.1371/journal.pone.0089966 e89966.
[57] S. Puwanun, R.M. Delaine-Smith, H.E. Colley, A simple rocker-induced mechanical stimulus upregulates mineralization by human osteoprogenitor cells in fibrous scaffolds, J. Tissue Eng. Reg. Med. 12 (2018) 370–381, https://doi.org/10.1002/term.2462.
[58] A.L. Olivares, E. Marsal, J.A. Planell, D. Lacroix, Finite element study of scaffold architecture design and culture conditions for tissue engineering, Biomaterials 30 (2009) 6142–6149, https://doi.org/10.1016/j.biomaterials.2009.07.041.
[59] P.J. Prendergast, R. Huiskes, K. Soballe, Biophysical stimuli on cells during tissue differentiation at implant interfaces, J. Biomech. 30 (1997) 539–548, https://doi.org/10.1016/s0021-9290(96)00140-6.
[60] V.I. Sikavitsas, G.N. Bancroft, J.J. Lemoine, M.A. Liebschner, M. Dauner, A. G. Mikos, Flow perfusion enhances the calcified matrix deposition of marrow stromal cells in biodegradable nonwoven fiber mesh scaffolds, Ann. Biomed. Eng. 33 (2005) 63–70, https://doi.org/10.1007/s10439-005-8963-x.
[61] V. Wu, M.N. Helder, N. Bravenboer, C.M. ten Bruggenkate, J. Jin, J. Klein-Nulend, E.A.J.M. Schulten, Bone tissue regeneration in the oral and maxillofacial region: a review on the application of stem cells and new strategies to improve vascularization, Stem Cell. Int. 2019 (2019) 1–15, https://doi.org/10.1155/2019/6279721.
[62] L. Figueiredo, R. Pace, C. D'Arros, G. Rethore, J. Guicheux, C. Le Visage, P. Weiss, Assessing glucose and oxygen diffusion in hydrogels for the rational design of 3D stem cell scaffolds in regenerative medicine, J. Tissue Eng. Reg. Med. 12 (2018) 1238–1246, https://doi.org/10.1002/term.2656.
[63] E. Volkmer, S. Otto, H. Polzer, M. Saller, D. Trappendreher, D. Zagar, S. Hamisch, G. Ziegler, A. Wilhelmi, W. Mutschler, M. Schieker, Overcoming hypoxia in 3D culture systems for tissue engineering of bone in vitro using an automated, oxygen-triggered feedback loop, J. Mater. Sci. Mater. Med. 23 (2012) 2793–2801, https://doi.org/10.1007/s10856-012-4725-0.
[64] C. Henrionnet, G. Liang, E. Roeder, M. Dossot, H. Wang, J. Magdalou, P. Gillet, A. Pinzano, Hypoxia for mesenchymal stem cell expansion and differentiation: the best way for enhancing TGF-induced chondrogenesis and preventing calcifications in alginate beads, Tissue Eng. 23 (2017) 913–922, https://doi.org/10.1089/ten.tea.2016.0426.
[65] C.K. Colton, Implantable biohybrid artificial organs, Cell Transplant. 4 (1995) 415–436, https://doi.org/10.1016/0963-6897(95)00025-s.
[66] A. Moya, J. Paquet, M. Deschepper, N. Larochette, K. Oudina, C. Denoeud, M. Bensidhoum, D. Logeart-Avramoglou, H. Petite, Human mesenchymal stem cell failure to adapt to glucose shortage and rapidly use intracellular energy reserves through glycolysis explains poor cell survival after implantation, Stem Cell. 36 (2018) 363–376, https://doi.org/10.1002/stem.2763.
[67] E. Volkmer, I. Drosse, S. Otto, A. Stangelmayer, M. Stengele, B.C. Kallukalam, W. Mutschler, M. Schieker, Hypoxia in static and dynamic 3D culture systems for tissue engineering of bone, Tissue Eng. 14 (2008) 1331–1340, https://doi.org/10.1089/ten.tea.2016.0426.
[68] S. Zhou, Z. Cui, J.P. Urban, Nutrient gradients in engineered cartilage: metabolic kinetics measurement and mass transfer modeling, Biotechnol. Bioeng. 101 (2008) 408–421, https://doi.org/10.1002/bit.21887.
[69] S.V. Komarova, F.I. Ataullakhanov, R.K. Globus, Bioenergetics and mitochondrial transmembrane potential during differentiation of cultured osteoblasts, Am. J. Physiol. Cell Physiol. 279 (2000) C1220–C1229, https://doi.org/10.1152/ajpcell.2000.279.4.c1220.
[70] M.J. Oedayrajsingh-Varma, S.M. van Ham, M. Knippenberg, M.N. Helder, J. Klein-Nulend, T.E. Schouten, M.J. Ritt, F.J. van Milligen, Adipose tissue-derived mesenchymal stem cell yield and growth characteristics are affected by the tissue-harvesting procedure, Cytotherapy 8 (2006) 166–177, https://doi.org/10.1080/14653240600621125.
[71] D.C. Chow, L.A. Wenning, W.M. Miller, E.T. Papoutsakis, Modeling pO(2) distributions in the bone marrow hematopoietic compartment. I. Krogh's model, Biophys. J. 81 (2001) 675–684, https://doi.org/10.1016/s0006-3495(01)75732-3.
[72] M.A. Fernandez-Seara, S.L. Wehrli, F.W. Wehrli, Diffusion of exchangeable water in cortical bone studied by nuclear magnetic resonance, Biophys. J. 82 (2002) 522–529, https://doi.org/10.1016/s0006-3495(02)75417-9.
[73] J.S. Tjia, P.V. Moghe, Regulation of cell motility on polymer substrates via "dynamic," cell internalizable, ligand microinterfaces, Tissue Eng. 8 (2002) 247–261, https://doi.org/10.1089/107632702753725012.
[74] J. Pierre, C. Oddou, Engineered bone culture in a perfusion bioreactor: a 2D computational study of stationary mass and momentum transport, Comput. Methods Biomech. Biomed. Eng. 10 (2007) 429–438, https://doi.org/10.1080/10255840701494635.
[75] S. Kou, L. Pan, D. van Noort, G. Meng, X. Wu, H. Sun, J. Xu, I. Lee, A multishear microfluidic device for quantitative analysis of calcium dynamics in osteoblasts, Biochem. Biophys. Res. Commun. 408 (2011) 350–355, https://doi.org/10.1016/j.bbrc.2011.04.044.
[76] R.M. Delaine-Smith, A. Sittichokechaiwut, G.C. Reilly, Primary cilia respond to fluid shear stress and mediate flow-induced calcium deposition in osteoblasts, Faseb. J. 28 (2014) 430–439.

Hadi Seddiqi: MSc, is chemical engineer. His current research is in the area of bone tissue engineering using FE modeling, with special focus on fluid mechanics and mass transfer.

Alireza Saatchi: MSc, chemical engineer, is PhD student at the University of Tehran and Vrije Universiteit Amsterdam. His work is on FE modeling for bone tissue engineering using bioreactors, scaffolds, and cells.

Prof.dr. Ghassem Amoabediny: PhD, is professor of Biochemical, Biomedical and NanoBioEngineering. His expertise is the design of new bioreactors for *e.g.* bone tissue engineering.

Dr. Marco N. Helder, PhD: is associate professor. His work on "Stem Cell Technology" is internationally leading. He performs translational research on bone tissue engineering and cell therapy.

Sonia Abbasi Ravasjani: MSc, is biochemical Engineer. Her current research is in the area of tissue engineering using biomaterials, with special focus on 3D scaffolds containing cells.

Mohammadreza Safari Hajat Aghaei: MSc, chemical engineer, is PhD student at the University of Isfahan. His work is on designing and optimizing bioreactors for bone tissue engineering.

Jianfeng Jin: DDS, MSc, is PhD student at ACTA. His research focuses on physico-chemical niche conditions of bone and muscle stem cells. He obtained data on NO produced by osteoblasts after mechanical loading.

Dr. Behrouz Zandieh-Doulabi: PhD, is senior scientist of Oral Cell Biology with special expertise in Molecular Biology. His work on "Regenerative Medicine" uses stem cells for bone tissue engineering.

Prof.dr. Jenneke Klein-Nulend, PhD, is professor of Oral Cell Biology. Her work on "Cell Biology of Bone Adaptation to Mechanical Loading and Bone Regeneration" is internationally leading.